ASTRONOMY & ASTROPHYSICS
SUPPLEMENT SERIES

OCTOBER II **1999**, PAGE 257

Astron. Astrophys. Suppl. Ser. **139**, 257–275 (1999)

Survey of bipolar outflows and methanol masers in the $C^{32}S$ (2 − 1) and $C^{34}S$ (2 − 1) lines in the Northern sky⋆

G.M. Larionov[1], I.E. Val'tts[1], A. Winnberg[2], L.E.B. Johansson[2], R.S. Booth[2], and V.V. Golubev[3]

[1] Astro Space Center of Lebedev Physical Institute, Profsoyuznaya 84/32, 117810 Moscow, Russia
[2] Onsala Space Observatory, S–439 92 Onsala, Sweden
[3] Moscow State University, Physical Faculty, Department of Astronomy, Universitetskii pr. 13, 119899 Moscow, Russia

Received February 25, 1998; accepted July 5, 1999

Abstract. A survey of 158 sources (bipolar outflows and methanol masers) was carried out in the CS(2 − 1) and $C^{34}S(2-1)$ lines to measure and compare densities in a large number of bipolar outflows and in Class I and Class II methanol masers, both associated with and unrelated to bipolar outflows. The statistical characteristics of the regions, forming Class I methanol masers differ from those both in the centres of bipolar outflows and in the regions forming Class II methanol masers. It is possible that physical conditions in bipolar outflows are closer to physical conditions of Class II methanol masers.

Key words: ISM: general — ISM: jets and outflows, molecules

1. Introduction

A bipolar outflow is a physical phenomenon which accompanies the process of star formation. This is the earliest phase of stellar evolution seen by observers. At the present time bipolar outflows are some of the most widely studied phenomena in astrophysics; the number of bipolar outflows detected thus far is more than 200. Their properties and characteristics have been described in detailed surveys, e.g. Bally & Lane (1991), Bachiller & Gómez-González (1992). The most complete catalogues of bipolar outflows were made by Fukui (1989), Xiang & Turner (1995), and Wu et al. (1996). Numerous observations show convincingly that flowing matter usually has a bipolar structure. Such flows have characteristics similar to those of young objects of all masses and luminosities.

Send offprint requests to: A. Winnberg

⋆ Figures i and ii are only available in electronic form at http://www.edpsciences.com

On the other hand, molecular maser activity often accompanies the process of star formation and is also a widespread phenomenon. Methanol masers as well as OH and H_2O masers, are often located close to young stellar objects, ultracompact HII regions, IR sources, HH objects, Bok globules, and other unusual objects, associated with regions of star formation. The influence of bipolar outflows on methanol maser activity has not been adequately studied, but some publications suggest a connection between methanol masers and bipolar outflows (Plambeck & Menten 1990; Haschick et al. 1990; Kalenskii et al. 1992). It has also been shown that the presence of bipolar outflows increases the abundance of methanol (Bachiller et al. 1995).

Some well studied regions of star formation have powerful bipolar outflows, but do not manifest methanol activity. In others, where both bipolar outflows and methanol masers coexist, the role of the central star's mass, age, the power of the flow, and other characteristics in maser excitation is unknown.

It is possible that methanol masers are formed in a gas disk surrounding a protostellar object, and interferometric observations show that methanol masers are associated with the centre of bipolar outflows (see e.g. Pratap & Menten 1992).

It is possible also that methanol masers are produced at a shock front, which results from the interaction between flow and molecular cloud (Johnston et al. 1992).

In both cases maser condensations are likely to be deeper imbedded in regions of very dense gas.

In this paper we present the results of a $J = 2 - 1$ CS and $C^{34}S$ survey of 158 sources (bipolar outflows and methanol masers). CS lines are indicators of very dense gas. These lines are excited by a density above the critical level $n_{\rm crit} = 10^4 - 10^7$ cm^{-3} (Snell et al. 1982; Snell et al. 1984; Mundy et al. 1986).

The present survey was carried out in order to derive some physical parameters (e.g. $N_{\rm CS}$ and τ) and compare densities in a large number of bipolar outflows and of Class I and Class II methanol masers (Menten 1987; Batrla et al. 1987), both associated with and unrelated to bipolar outflows.

1.1. Important surveys in CS lines

Observations of CS lines in HII regions and dark clouds have been done in the following works:

Turner et al. (1973) surveyed interstellar objects in the (1−0) and (2−1) transitions of the CS and $C^{34}S$ lines. The CS line was detected in 19 out of 26 sources. $C^{34}S$ was detected in 5 out of the positive 19 CS sources: W3(OH), Ori A, Sgr B2, W51, and DR21(OH).

Liszt & Linke (1975) surveyed five molecular clouds associated with HII regions in the CS(1−0), (2−1), and (3−2) lines.

Linke & Goldsmith (1980) surveyed 32 molecular clouds in the CS(2−1) and (1−0) lines.

Plume et al. (1992) surveyed 179 regions of star formation in the CS(7−6) line, selected in accordance with the criterion for the existence of H_2O masers close to the star forming regions. The CS(7−6) emission line was detected in 104 sources.

Zinchenko et al. (1994) surveyed the CS(2−1) and $C^{34}S$(2−1) lines in 11 molecular cloud cores, associated with regions of star formation.

Wolf-Chase et al. (1995) surveyed 10 outflows and 30 IRAS sources in the Mon OB1 dark cloud in the CS(2−1), (5−4), and (7−6) lines.

Juvela (1996) surveyed 33 southern molecular cores associated with H_2O masers in several CS and $C^{34}S$ lines. The clouds have been mapped mainly in the CS(2−1), CS(5−4), and $C^{34}S$(2−1) lines. All central positions of the clouds have been observed in both isotopomers in the transitions $J = 3 - 2$ and 5−4 as well as in $C^{34}S$(2−1). Some selected clouds were also mapped in CS(3−2). CS(7−6) was observed in 14 and $C^{34}S$(7−6) in seven clouds.

Bronfman et al. (1996) carried out a CS(2−1) survey of IRAS point sources in the Galactic plane. Sources were selected according to a colour criterion. In 843 sources out of 1427 the CS(2−1) line was observed successfully.

Anglada et al. (1996) surveyed 172 regions of star formation, which areassociated with H_2O masers. Observations were carried out to compare the width of lines detected in the directions of H_2O masers and in the other directions.

Plume et al. (1997) surveyed 150 regions of massive star formation in the CS(5−4), (3−2), and (2−1) transitions and in the same transitions of $C^{34}S$ selected by the presence of an H_2O maser.

A few star formation regions were observed in the CS(2−1) and (1−0) lines by other authors (Bally 1982; Zhou et al. 1991; Ohashi et al. 1991; Pastor et al. 1991; Churchwell et al. 1992). In spite of numerous CS surveys there is no one which was devoted to comparison of properties of bipolar outflows and methanol masers.

2. Observations

The observations were carried out in the period from May 14 to May 31, 1995, with the 20−m radio telescope in Onsala (Sweden). The rest frequency of the CS(2−1) line is 97980.968 MHz and that of the $C^{34}S$(2−1) line is 96412.982 MHz (Lovas 1992). The aperture efficiency is $47 \pm 3\%$ and the half−power beam width is $39''$ at 98 GHz. The pointing accuracy is $3''$ rms in azimuth and elevation. The beam efficiency $\eta_{\rm mb} = 0.56$. The observations were performed in a frequency-switching mode with a 12-MHz frequency throw. A cryogenically cooled low-noise SIS mixer was used as receiver frontend. The system noise temperature, corrected for atmospheric absorption, rear ward spillover and radome losses, varied during observations between 250 and 500 K, depending on weather conditions and elevation of the sources. The data were calibrated using the standard chopper-wheel method of Kutner & Ulich (1981). An antenna temperature of 1 K corresponds to 18.7 Jy. The backend was a 64 MHz-wide 256-channel filter spectrometer with a frequency resolution of 250 kHz (velocity resolution 0.7 km s^{-1} at 98 GHz).

3. Results

Observations of 158 sources were successfully carried out (111 bipolar outflows, 26 Class I methanol masers, and 47 Class II methanol masers − some objects are methanol masers of Class I and II simultaneously or bipolar outflow and methanol masers). Of the 158 sources, 149 were detected in the CS(2−1) line (97 bipolar outflows, 26 Class I methanol masers, 45 Class II methanol masers). Of these 149 sources, 51 were observed in the $C^{34}S$ line. The list of bipolar outflows was compiled from the catalogues of Fukui (1989) and Xiang & Turner (1995). The list of Class I methanol masers was compiled from the following surveys: Haschick et al. (1990), Bachiller et al. (1990), Kalenskii et al. (1992), Kalenskii et al. (1994). The list of Class II methanol masers was compiled from the surveys of Menten (1991) and Slysh et al. (1998).

At the present time 27 strong Class I methanol masers with a flux ≥ 50 Jy at 44 GHz are known. It is possible to observe 14 of them at Onsala. Some well known masers were left out of our survey, such as Ori KL, OMC–2, and DR21(OH), but some were included for comparison. Of the remaining 11, only 7 were observed, because of weather conditions. The other 19 Class I methanol masers of our list have a lower flux at 44 GHz. We will call a CS line with an integrated intensity > 10 K km s^{-1},

Table 1. Line parameters determined from CS(2−1) and $C^{34}S$(2−1) observations

Source name or IRAS name	α_{1950} (h m s)	δ_{1950} (° ′ ″)	Line components	Area (K km s^{-1})	$V_{\rm lsr}$ (km s^{-1})	ΔV (km s^{-1})	$T_{\rm A}^{*}$ (K)	Source type
LkHα 198	00 08 47.9	58 33 09	1	0.5(0.1)	0.3(0.1)	1.4(0.2)	0.4	BO
00213+6530	00 21 22.0	65 30 25	1	0.7(0.1)	−21.5(0.3)	3.2(0.9)	0.2	BO
			2	1.1(0.1)	−19.6(0.1)	2.3(0.3)	0.5	
00259+6510	00 25 59.8	65 10 12	1	1.4(0.1)	−17.2(0.1)	1.9(0.1)	0.7	BO
L1293	00 37 57.4	62 48 26	1	2.6(0.1)	−17.6(0.1)	2.0(0.1)	1.3	BO
NGC 281−W	00 49 27.8	56 17 28	1	2.2(0.4)	−28.5(0.1)	15.6(2.0)	0.1	MMII, BO
			2	12.2(0.4)	−30.7(0.1)	5.0(0.1)	2.3	
			1*	0.1(0.1)	−34.9(0.4)	1.6(1.1)	0.1 d	
			2*	1.3(0.1)	−30.9(0.1)	3.7(0.3)	0.3	
NGC 281−E	00 51 18.0	56 17 07	1	1.3(0.2)	−29.7(0.2)	4.2(0.5)	0.3	BO
			2	0.9(0.2)	−30.3(0.1)	1.5(0.2)	0.6	
S187−IRS	01 19 58.0	61 33 08	1	0.5(0.1)	−13.4(0.1)	1.6(0.2)	0.3	BO
IC1805−W	02 25 14.5	61 20 10	1	4.4(0.2)	−50.3(0.3)	10.3(0.7)	0.4	BO
			2	1.9(0.2)	−51.5(0.1)	1.9(0.1)	0.9	
			1*	0.1(0.1)	−51.6(0.1)	0.8(1.4)	0.2	
RNO13	03 22 04.7	30 35 49	1	0.9(0.1)	3.7(0.3)	5.2(0.7)	0.2	BO
			2	0.4(0.1)	3.7(0.1)	1.3(0.2)	0.3	
L1448(U−Star)	03 22 33.5	30 33 34	1	0.6(0.2)	9.0(0.9)	5.2(2.0)	0.1	BO
			2	2.1(0.2)	4.9(0.1)	2.1(0.1)	1.0	
L1455−M	03 24 22.0	30 05 24	1	0.9(0.2)	7.1(0.6)	5.6(0.7)	0.2	BO
			2	0.9(0.1)	5.3(0.1)	1.4(0.1)	0.6	
L1455 (RNO15FIR)	03 24 34.9	30 02 36	1	2.9(0.1)	5.2(0.1)	2.4(0.1)	1.2	BO
			1*	0.2(0.1)	2.5(0.5)	2.1(1.0)	0.1	
			2*	0.2(0.1)	4.9(0.1)	0.8(1.1)	0.2	
L1455−NW	03 25 00.0	30 00 00	1	0.9(0.1)	5.3(0.1)	1.9(0.2)	0.4	BO
LkHα 325	03 25 47.8	30 34 43	1	1.4(0.1)	5.0(0.2)	8.0(0.6)	0.2	BO
			2	0.4(0.1)	5.9(0.1)	1.4(0.2)	0.3	BO
03262+3108	03 26 14.7	31 08 16	1	1.2(0.2)	7.8(0.3)	4.5(0.6)	0.2	BO
			2	0.8(0.2)	8.7(0.1)	1.0(0.3)	0.7	
T Tau	04 19 02.4	19 25 00	1	1.1(0.1)	8.5(0.1)	1.6(0.1)	0.6	BO
04191+1523	04 19 08.5	15 23 16	1	0.3(0.1)	1.3(0.2)	2.6(0.4)	0.1	BO
			2	1.0(0.1)	7.1(0.1)	4.2(0.4)	0.2	
			3	0.3(0.1)	6.9(0.1)	0.8(0.1)	0.3	
L1524 (HARO 6−10)	04 26 21.7	24 26 26	1	1.3(0.1)	6.4(0.1)	1.8(0.1)	0.7	BO
04269+3108	04 26 54.5	35 07 57	1	0.3(0.1)	0.6(0.2)	1.5(0.4)	0.2	BO
L1529 (TMC−2)	04 29 43.4	24 13 54	1	0.8(0.1)	6.7(0.1)	1.4(0.2)	0.5	BO
IC2087	04 36 54.6	25 39 17	1	0.3(0.1)	6.7(0.1)	1.7(0.2)	0.2	BO
L1634	05 17 21.9	−05 55 05	1	1.5(0.1)	8.3(0.1)	1.4(0.1)	1.0	BO
RNO43	05 29 38.0	12 51 08	1	0.6(0.1)	11.4(0.3)	5.1(0.7)	0.1	BO
RNO43−N	05 29 38.0	12 55 08	1	1.3(0.1)	10.6(0.1)	3.9(0.2)	0.3	BO
RNO43IRS2	05 30 05.3	12 51 08	1	0.4(0.1)	10.3(0.2)	1.9(0.4)	0.2	BO
Ori A−W	05 30 14.5	−05 37 52	1	1.3(0.4)	10.3(0.8)	6.1(1.1)	0.2	BO
			2	1.7(0.3)	8.6(0.1)	2.0(0.3)	0.8	
05329−0512	05 32 58.7	−05 12 11	1	4.8(0.3)	11.1(0.1)	4.6(0.2)	1.0	BO
			2	6.7(0.3)	11.3(0.1)	1.6(0.1)	3.8	
			1*	1.0(0.1)	11.4(0.1)	2.4(0.4)	0.4	
L1641−N	05 33 52.7	−06 24 02	1	2.7(0.5)	8.6(0.4)	4.7(0.3)	0.5	BO
			2	4.6(0.5)	7.2(0.1)	2.2(0.1)	2.0	
			1*	0.4(0.1)	7.4(0.4)	2.2(0.6)	0.2	
NGC 1999	05 33 59.4	−06 44 45	1	0.6(0.2)	12.5(0.7)	3.5(1.0)	0.2	BO
			2	1.8(0.3)	8.9(0.2)	3.0(0.3)	0.6	
AFGL5157	05 34 32.6	31 57 40	1	0.7(0.1)	−17.8(0.1)	2.7(0.3)	0.2	BO

Table 1. continued

Source name or IRAS name	α_{1950} (h m s)	δ_{1950} (° ′ ″)	Line components	Area (K km s^{-1})	$V_{\rm lsr}$ (km s^{-1})	ΔV (km s^{-1})	$T_{\rm A}^{*}$ (K)	Source type
Ori I−2	05 35 33.2	−01 46 50	1	0.2(0.1)	11.8(0.3)	2.1(0.6)	0.1	BO
			2	0.7(0.1)	13.0(0.1)	0.8(0.3)	0.9	
S233	05 35 48.8	35 43 41	1	7.1(0.7)	−17.1(0.2)	7.7(0.7)	0.9	BO
			2	5.3(0.7)	−17.4(0.1)	2.7(0.2)	1.8	
			1*	0.8(0.2)	−24.9(0.6)	5.5(1.2)	0.1 d	
			2*	1.7(0.2)	−17.6(0.3)	5.5(0.6)	0.3	
S231	05 35 51.3	35 44 16	1	14.0(0.2)	−16.5(0.1)	5.4(0.1)	2.5	MMI, MMII
			1*	1.5(0.1)	−17.2(0.2)	4.4(0.4)	0.3	
L1641−C	05 36 20.9	−07 02 43	1	1.5(0.2)	4.4(0.2)	4.1(0.3)	0.4	BO
			2	0.9(0.2)	3.4(0.1)	1.5(0.2)	0.6	
GGD 4	05 37 21.3	23 49 22	1	4.7(0.4)	2.8(0.2)	9.5(0.6)	0.5	BO
			2	2.9(0.3)	2.1(0.1)	3.3(0.2)	0.8	
S235B	05 37 31.0	35 39 55	1	7.9(0.6)	−16.2(0.2)	8.3(0.5)	0.9	MMI, BO
(GGD 5)			2	19.5(0.6)	−16.5(0.1)	2.9(0.1)	6.4	
			1*	1.1(0.1)	−16.9(0.1)	2.4(0.2)	0.4	
L1641−S3	05 37 31.1	−07 31 59	1	1.0(0.2)	5.8(0.3)	6.4(0.8)	0.1	BO
			2	0.5(0.1)	5.3(0.1)	2.4(0.3)	0.2	
L1641−S	05 38 02.7	−07 28 59	1	1.2(0.1)	4.6(0.1)	2.3(0.2)	0.5	BO
L1641−S4	05 38 24.6	−08 08 20	1	1.4(0.1)	5.5(0.1)	1.6(0.1)	0.8	BO
L1641−S2	05 40 23.2	−08 18 26	1	1.0(0.1)	3.1(0.1)	1.3(0.1)	0.7	BO
HH26IR	05 43 31.1	−00 15 28	1	1.2(0.2)	10.0(0.3)	6.6(1.2)	0.2	BO
			2	1.9(0.2)	10.5(0.1)	1.8(0.1)	1.1	
HH24	05 43 34.2	−00 11 08	1	3.6(0.1)	9.9(0.1)	1.9(0.1)	1.8	BO
NGC 2068 H_2O	05 43 58.0	−00 04 00	1	4.3(0.2)	8.0(0.2)	6.4(0.2)	0.6	BO
			2	1.9(0.2)	10.4(0.1)	1.9(0.1)	1.0	
S242	05 49 05.2	26 58 52	1	0.8(0.2)	0.5(0.1)	1.6(0.2)	0.5	
			2	1.2(0.2)	1.7(0.3)	3.9(0.3)	0.9	BO
L1617	05 49 09.1	02 47 48	1	1.0(0.2)	8.6(0.2)	3.4(0.6)	0.3	BO
			2	0.8(0.1)	8.7(0.1)	0.8(2.2)	0.9	
L1598−NW	05 49 27.9	08 20 48	1	0.7(0.1)	11.6(0.1)	1.3(0.1)	0.5	BO
L1598	05 49 39.1	08 12 55	1	0.7(0.1)	12.2(0.5)	5.7(0.8)	0.1	BO
			2	0.9(0.1)	11.3(0.1)	1.4(0.2)	0.6	
AFGL5180	06 05 53.9	21 38 57	1	10.5(0.6)	4.2(0.1)	9.3(0.4)	1.1	BO
			2	12.8(0.6)	3.3(0.1)	3.3(0.1)	3.7	
			1*	1.1(0.1)	3.1(0.1)	2.5(0.2)	0.4	
G188.9+0.9	06 05 54.0	21 39 09	1	5.3(0.7)	3.4(0.1)	6.8(0.5)	0.7	MMII
			2	7.6(0.7)	3.2(0.1)	3.3(0.1)	2.2	
GGD 12−15	06 08 24.5	−06 11 12	1	6.2(0.4)	11.0(0.1)	5.6(0.3)	1.0	BO
			2	5.2(0.4)	11.7(0.1)	2.3(0.1)	2.1	
			1*	1.6(0.1)	11.1(0.1)	3.0(0.4)	0.5	
S254−258	06 09 57.9	18 00 12	1	7.2(0.4)	7.5(0.1)	7.8(0.4)	0.9	MMII, BO
			2	9.6(0.5)	7.5(0.1)	2.8(0.1)	3.2	
			1*	1.2(0.3)	7.7(0.2)	3.4(0.6)	0.4	
			2*	0.7(0.3)	7.3(0.1)	1.3(0.4)	0.5	
Mon R2−E	06 10 21.8	−06 12 28	1	1.1(0.1)	10.9(0.4)	7.9(0.8)	0.1	BO
(GGD 16−17)			2	1.6(0.1)	12.4(0.1)	2.0(0.1)	0.8	
S255	06 10 01.0	18 00 44	1	3.8(0.1)	7.5(0.1)	3.3(0.1)	1.1	MMI, MMII
			1*	1.1(0.2)	7.3(0.3)	4.4(0.8)	0.2	
RNO73	06 30 52.7	04 02 27	1	0.3(0.1)	15.5(0.8)	3.9(0.8)	0.7	BO
			2	0.4(0.1)	15.3(0.8)	1.9(0.8)	0.2	
R Mon	06 36 25.6	08 46 57	1	0.3(0.1)	9.4(0.2)	1.5(0.3)	0.2	BO

Table 1. continued

Source name or IRAS name	α_{1950} (h m s)	δ_{1950} (° ′ ″)	Line components	Area (K km s^{-1})	$V_{\rm lsr}$ (km s^{-1})	ΔV (km s^{-1})	$T_{\rm A}^{*}$ (K)	Source type
Mon OB1−D	06 38 17.8	09 39 03	1	4.3(0.6)	5.1(0.2)	5.5(0.6)	0.7	BO
			2	3.1(0.6)	5.2(0.1)	2.1(0.2)	1.4	
Mon OB1−I	06 38 19.0	10 52 39	1	3.9(0.3)	11.6(0.1)	7.1(0.4)	0.5	BO
			2	5.2(0.3)	11.6(0.1)	2.8(0.1)	1.8	
Mon OB1−G	06 38 27.0	09 58 28	1	0.4(0.1)	4.7(0.1)	1.3(0.3)	0.3	BO
NGC 2264(IR)	06 38 28.0	09 32 12	1	5.3(0.8)	9.0(0.8)	5.0(0.8)	1.0	MMI, MMII
			2	11.2(0.8)	7.6(0.8)	3.1(0.1)	3.4	
			1*	1.5(0.2)	7.6(0.1)	2.9(0.4)	0.5	
S287−N	06 45 19.2	−02 09 32	1	1.2(0.1)	27.3(0.1)	2.0(0.2)	0.5	BO
BFS56	06 56 45.1	−03 50 41	1	2.3(0.1)	26.6(0.1)	2.5(0.2)	0.9	BO
L1654	06 57 16.8	−07 42 16	1	0.2(0.1)	13.6(0.2)	1.0(0.4)	0.2	BO
G9.62+0.19	18 03 16.0	−20 32 01	1	7.0(0.7)	4.5(0.8)	12.7(0.8)	0.5	MMII
			2	13.2(0.7)	5.3(0.8)	6.9(0.8)	1.8	
G11.91−0.15	18 09 18.1	−18 42 25	1	1.2(0.2)	44.5(0.4)	4.4(0.7)	0.3	MMII
G12.22−0.12	18 09 45.0	−18 25 10	1	6.9(0.2)	25.3(0.1)	6.5(0.2)	1.0	MMII
W33B	18 10 59.3	−18 02 40	1	3.0(0.1)	58.1(0.1)	4.0(0.2)	0.7	MMII
W33−Met	18 11 15.7	−17 56 53	1	41.5(0.3)	35.7(0.1)	7.8(0.1)	5.0	MMI
			1*	1.6(0.5)	32.1(0.3)	2.5(0.7)	0.6 d	
			2*	3.5(0.5)	35.9(0.3)	3.9(0.6)	0.9	
W33A	18 11 44.5	−17 52 56	1	6.3(0.5)	38.8(0.8)	15.7(0.8)	0.4	MMII
			2	9.6(0.5)	36.7(0.8)	6.7(0.8)	1.3	
			1*	0.5(0.3)	34.2(0.3)	1.4(0.5)	0.3 d	
			2*	6.7(0.6)	37.5(0.3)	7.0(0.7)	0.9	
18128−1640	18 12 51.1	−16 39 53	1	3.8(0.3)	10.1(0.3)	6.3(0.6)	0.6	MMII
L483	18 14 50.6	−04 40 49	1	0.4(0.3)	5.3(0.7)	2.7(1.2)	0.2	BO
			2	0.3(0.2)	5.5(0.1)	0.8(5.2)	0.4	
G18.46−0.01	18 21 48.0	−12 53 02	1	1.7(0.2)	50.7(0.1)	2.5(0.3)	0.6	MMII
G19.61−0.23	18 24 50.3	−11 58 34	1	11.8(0.1)	42.4(0.1)	9.2(0.1)	1.2	MMI, MMII
			1*	3.2(0.2)	41.6(0.2)	7.8(0.5)	0.4	
G20.24+0.08	18 24 55.8	−11 16 24	1	1.8(0.4)	71.9(0.2)	1.7(0.5)	1.0	MMII
L379IRS3	18 26 32.9	−15 17 51	1	12.0(0.4)	17.8(0.1)	6.6(0.2)	1.7	MMI, MMII, BO
L379IRS2	18 27 43.4	−15 16 45	1	8.7(0.6)	19.1(0.3)	12.4(1.0)	0.7	BO
			2	2.3(0.4)	19.5(0.1)	2.8(0.4)	0.8	
18316−0608	18 31 39.0	−06 08 08	1	0.6(0.1)	54.8(0.1)	0.8(0.4)	0.8	MMII
G23.01−0.41	18 31 56.7	−09 03 18	1	1.6(0.2)	74.8(0.2)	3.2(0.4)	0.4 d	MMII
			2	0.6(0.1)	78.7(0.1)	1.4(0.3)	0.5	
G24.33+0.11	18 32 32.3	−07 38 24	1	2.6(0.3)	112.0(0.3)	6.0(0.6)	0.4	MMII
W42	18 33 30.3	−07 14 42	1	7.6(0.2)	111.0(0.1)	5.6(0.2)	1.3	MMI
			1*	2.5(0.1)	110.0(0.1)	5.1(0.2)	0.5	
18379−0500	18 37 55.5	−05 00 34	1	7.1(0.4)	32.1(0.2)	7.0(0.5)	1.0	MMII
G27.35−0.20	18 39 16.0	−05 06 35	1	0.8(0.1)	97.0(0.3)	3.3(0.6)	0.2	MMII
G28.21−0.05	18 40 21.6	−04 16 26	1	5.5(0.2)	96.8(0.1)	7.2(0.3)	0.7	MMII
G28.83−0.25	18 42 12.4	−03 49 08	1	4.5(0.2)	87.3(0.1)	5.6(0.3)	0.8	MMII
G30.70−0.06	18 44 58.9	−02 04 07	1	7.9(0.3)	88.8(0.1)	6.1(0.3)	1.2 d	MMII
			2	3.5(0.3)	96.2(0.2)	4.7(0.4)	0.7	
			1*	0.9(0.3)	87.6(0.4)	2.3(0.7)	0.4 d	
			2*	2.5(0.4)	91.6(0.3)	4.0(0.7)	0.6	
G30.82+0.28	18 44 00.5	−01 48 29	1	0.6(0.1)	92.7(0.3)	2.3(0.6)	0.3	MMII
			2	1.5(0.2)	97.6(0.2)	3.6(0.4)	0.4	
G30.79−0.06	18 45 08.8	−01 59 12	1	3.2(0.2)	93.9(0.3)	8.2(0.5)	0.4	MMII
G30.80−0.10	18 45 11.0	−01 57 57	1	1.0(0.2)	91.9(0.8)	3.7(0.8)	0.3 tr	MMI
			2	3.1(0.2)	95.4(0.8)	2.7(0.8)	1.1	
			3	1.3(0.2)	100.0(0.8)	4.3(0.8)	0.3	

Table 1. continued

Source name or IRAS name	α_{1950} (h m s)	δ_{1950} (° ′ ″)	Line components	Area (K km s^{-1})	$V_{\rm lsr}$ (km s^{-1})	ΔV (km s^{-1})	$T_{\rm A}^{*}$ (K)	Source type
			1*	2.0(0.1)	97.1(0.3)	9.7(0.7)	0.2	
W43M	18 45 36.8	−01 29 12	1	0.7(0.3)	105.0(1.0)	4.5(2.6)	0.1	MMII
			2	0.5(0.2)	109.0(0.2)	1.9(0.6)	0.3	
G33.13−0.09	18 49 33.6	00 04 25	1	1.3(0.2)	74.2(0.2)	3.1(0.4)	0.4 d	MMII
			2	2.2(0.3)	78.1(0.2)	4.0(0.5)	0.5	
18497+0022	18 49 46.9	00 22 07	1	3.1(0.3)	74.6(0.2)	9.5(0.7)	0.3	MMII
			2	2.2(0.3)	75.1(0.1)	3.5(0.2)	0.6	
			1*	2.1(0.4)	73.0(0.5)	5.4(1.1)	0.4	
G34.26+0.16	18 50 46.1	01 11 12	1	23.8(0.2)	57.0(0.1)	4.7(0.1)	4.8 d	MMI, MMII
			2	3.2(0.2)	63.3(0.1)	3.3(0.2)	0.9	
			1*	2.9(0.7)	57.9(1.0)	4.3(0.3)	0.6	
			2*	0.2(0.4)	63.2(0.8)	2.1(0.3)	0.1 d	
G35.03+0.35	18 51 30.3	01 57 30	1	2.7(0.3)	52.5(0.2)	8.1(0.8)	0.3	MMII
			2	2.4(0.3)	52.9(0.1)	3.1(0.2)	0.7	
			1*	0.8(0.1)	52.7(0.1)	1.6(0.2)	0.4	
G35.05−0.52	18 54 37.1	01 35 01	1	2.6(0.1)	50.5(0.1)	3.6(0.1)	0.7	MMI
			1*	1.1(0.1)	50.5(0.1)	3.4(0.3)	0.3	
18572+0057	18 57 16.2	00 57 20	1	1.6(0.1)	46.3(0.1)	4.3(0.3)	0.4	MMII
W48	18 59 13.8	01 09 20	1	8.4(0.1)	43.9(0.1)	5.7(0.1)	1.4	MMII
			1*	6.3(0.4)	43.1(0.3)	9.1(0.7)	0.7	
G40.62−0.14	19 03 34.9	06 41 55	1	5.3(0.1)	32.9(0.1)	5.4(0.1)	0.9	MMII
			1*	0.5(0.1)	25.6(0.8)	2.7(0.8)	0.2 tr	
			2*	1.0(0.1)	29.2(0.8)	2.8(0.8)	0.4	
			3*	0.8(0.1)	32.3(0.8)	2.4(0.8)	0.3	
W49	19 07 51.7	09 01 11	1	8.8(0.3)	2.8(0.1)	7.3(0.2)	1.1 d	MMI, MMII, BO
			2	17.3(0.3)	12.1(0.1)	8.2(0.2)	2.0	
			1*	5.8(0.2)	11.4(0.2)	10.5(0.5)	0.5	
G43.80−0.13	19 09 30.8	09 30 47	1	4.5(0.2)	42.4(0.1)	6.0(0.3)	0.7	MMII
			2	4.9(0.2)	45.7(0.1)	5.3(0.2)	0.9	
			1*	6.4(0.5)	41.5(0.4)	10.0(0.8)	0.6	
G45.07+0.13	19 11 00.4	10 45 43	1	5.5(0.5)	58.0(0.3)	10.0(0.4)	0.5	MMII
			2	6.3(0.5)	59.6(0.1)	4.4(0.2)	1.3	
			1*	1.1(0.1)	58.7(0.2)	4.8(0.5)	0.2	
G45.47+0.13	19 11 47.5	11 07 14	1	4.8(0.1)	61.8(0.1)	5.5(0.1)	0.8	MMII
G45.47+0.05	19 12 04.4	11 04 11	1	2.0(0.2)	56.4(0.3)	7.0(0.8)	0.3	MMII
			2	8.4(0.2)	62.1(0.1)	6.7(0.2)	1.2	
			1*	1.5(0.1)	60.9(0.2)	5.4(0.5)	0.3	
L673	19 18 08.0	11 14 00	1	5.7(0.1)	5.8(0.1)	10.3(0.3)	0.5	BO
W51	19 21 24.4	14 24 48	1	19.0(2.2)	61.2(0.8)	20.3(0.8)	0.9	MMII
			2	63.4(2.1)	59.0(0.8)	9.9(0.8)	6.0	
W51−Met1	19 21 26.2	14 23 32	1	29.8(0.2)	56.3(0.1)	8.6(0.1)	3.3 d	MMI
			2	5.7(0.2)	67.7(0.1)	6.6(0.2)	0.8	
			1*	2.8(0.1)	55.5(0.2)	7.3(0.4)	0.4	
W51 e1/e2	19 21 26.2	14 24 43	1	106.0(0.7)	57.2(0.1)	10.3(0.1)	9.6	MMI
			1*	8.7(0.2)	57.1(0.1)	9.3(0.3)	0.9	
W51−Met2	19 21 28.8	14 23 47	1	25.7(0.2)	56.3(0.1)	9.2(0.1)	2.6 d	MMI
			2	1.8(0.1)	68.1(0.1)	3.2(0.2)	0.5	
			1*	3.7(0.1)	55.5(0.1)	6.3(0.2)	0.6	
W51−Met3	19 21 27.5	14 23 52	1	52.1(0.2)	56.5(0.1)	10.4(0.1)	4.7 d	MMI
			2	5.0(0.2)	68.2(0.1)	4.9(0.2)	1.0	
W51−Met4	19 21 25.6	14 25 41	1	1.5(0.1)	51.3(0.1)	2.8(0.2)	0.5 d	MMI

Table 1. continued

Source name or IRAS name	α_{1950} (h m s)	δ_{1950} (° ′ ″)	Line components	Area (K km s^{-1})	$V_{\rm lsr}$ (km s^{-1})	ΔV (km s^{-1})	$T_{\rm A}^{*}$ (K)	Source type
W51−Met3	19 21 27.5	14 23 52	1	52.1(0.2)	56.5(0.1)	10.4(0.1)	4.7 d	MMI
			2	5.0(0.2)	68.2(0.1)	4.9(0.2)	1.0	
W51−Met4	19 21 25.6	14 25 41	1	1.5(0.1)	51.3(0.1)	2.8(0.2)	0.5 d	MMI
			2	14.2(0.1)	61.8(0.1)	5.5(0.1)	2.4	
			1*	2.7(0.1)	61.9(0.1)	5.9(0.3)	0.4	
W51−Met5	19 21 20.5	14 24 12	1	3.8(0.2)	51.4(0.1)	4.6(0.3)	0.8 d	MMI
			2	36.0(0.3)	64.5(0.1)	11.8(0.1)	2.9	
			1*	1.9(0.1)	66.0(0.2)	7.2(0.4)	0.2	
W51M	19 21 36.2	14 24 43	1	9.6(0.2)	59.6(0.1)	10.3(0.2)	0.9 d	MMI
			2	2.0(0.2)	62.1(0.1)	3.5(0.2)	0.5	
			1*	1.0(0.1)	60.7(0.3)	6.4(1.9)	0.3	
L810	19 43 21.7	27 43 37	1	5.6(0.1)	16.6(0.1)	5.3(0.1)	1.0	BO
19589+3320	19 58 57.0	33 20 47	1	0.5(0.6)	−21.7(1.4)	2.6(1.6)	0.2	MMII
			2	0.5(0.5)	−20.5(0.1)	1.3(0.6)	0.3	
ON1	20 08 09.9	31 22 42	1	1.8(0.4)	5.8(0.8)	9.2(0.8)	0.2	MMI, MMII, BO
			2	9.3(0.4)	11.6(0.8)	5.9(0.8)	1.5	
			1*	1.7(0.1)	10.3(0.8)	11.4(0.8)	0.3	
20126+4104	20 12 41.0	41 04 20	1	4.7(0.4)	−3.2(0.1)	6.1(0.4)	0.7	BO
			2	2.3(0.4)	−3.4(0.1)	2.3(0.2)	0.9	
			1*	1.4(0.1)	−7.3(0.8)	8.3(0.8)	0.2	
			2*	2.1(0.1)	−3.2(0.8)	8.9(0.8)	0.2	
ON2	20 19 50.0	37 16 30	1	21.4(0.1)	−0.1(0.1)	8.0(0.1)	2.5	MMI, MMII
			1*	1.2(0.1)	−0.2(0.1)	5.1(0.3)	0.2	
AFGL2591	20 27 35.2	40 01 09	1	9.7(0.2)	−6.2(0.1)	5.0(0.1)	1.8	BO
W75N	20 36 51.1	42 27 20	1	16.5(0.2)	9.5(0.1)	4.4(0.1)	3.2	MMI, MMII, BO
			1*	1.5(0.5)	8.2(0.9)	6.5(0.9)	0.2	
			2*	0.9(0.4)	9.7(0.2)	2.1(0.7)	0.4	
DR21−West	20 37 07.6	42 08 46	1	11.4(0.4)	−4.2(0.2)	11.2(0.4)	1.0	MMI
			2	5.8(0.4)	−2.6(0.1)	3.6(0.2)	1.5	
			1*	0.8(0.4)	−6.5(0.8)	3.8(1.4)	0.2 d	
			2*	1.4(0.6)	−2.6(0.4)	3.6(0.8)	0.4	
DR21−Met C	20 37 12.6	42 08 46	1	14.1(0.5)	−2.0(0.1)	11.0(0.4)	1.2	MMI
			2	11.8(0.5)	−2.3(0.1)	3.8(0.1)	3.0	
			1*	1.5(0.2)	−3.2(0.5)	6.9(0.9)	0.2	
			2*	0.6(0.2)	−2.1(0.2)	2.1(0.4)	0.3	
L1036	20 37 43.1	56 58 56	1	0.3(0.1)	−2.7(0.1)	1.5(0.3)	0.2	BO
L1157	20 38 39.6	67 51 33	1	1.3(0.2)	2.7(0.2)	4.3(0.7)	0.3	BO
			2	0.3(0.2)	2.4(0.1)	1.1(0.3)	0.3	
PVCep	20 45 23.6	67 46 36	1	0.5(0.1)	2.3(0.6)	5.8(1.1)	0.1	BO
			2	0.3(0.1)	2.9(0.1)	1.0(0.4)	0.3	
V1057Cyg	20 57 06.2	44 03 47	1	0.8(0.1)	4.3(0.1)	1.4(0.1)	0.5	BO
L1228	20 58 14.5	77 24 05	1	1.6(0.1)	−8.0(0.2)	8.4(0.7)	0.2	BO
			2	0.8(0.1)	−8.0(0.1)	1.4(0.1)	0.5	
V1331Cyg	20 59 32.3	50 09 53	1	0.3(0.2)	1.3(0.8)	1.7(1.1)	0.2	BO
			2	0.5(0.3)	0.3(0.1)	0.8(0.4)	0.6	
L988−a	21 00 44.9	49 51 13	1	1.0(0.2)	0.8(0.1)	1.5(0.2)	0.6 d	BO
			2	0.9(0.2)	5.2(0.7)	5.3(1.7)	0.2	
L988−e	21 02 19.6	50 02 40	1	0.8(0.2)	−2.0(0.1)	2.0(0.3)	0.4	BO
IC1396W	21 24 38.7	57 43 14	1	0.8(0.1)	3.5(0.4)	5.1(0.9)	0.1	BO
			2	2.6(0.1)	0.5(0.1)	3.0(0.2)	0.8	
V645Cyg	21 38 11.3	50 00 45	1	2.2(0.1)	−43.9(0.1)	6.4(0.3)	0.3	BO,MMII
(GL2789)			2	2.0(0.1)	−43.9(0.1)	2.3(0.1)	0.8	
			1*	0.8(0.2)	−44.3(0.4)	3.3(0.4)	0.2	
NGC7129	21 41 52.0	65 49 50	1	1.2(0.1)	−9.9(0.1)	1.7(0.1)	0.7	BO
R146	21 42 40.0	65 52 57	1	0.2(0.1)	−9.5(0.1)	1.4(0.2)	0.2	MMI
IC1396E	21 44 30.8	57 12 29	1	0.7(0.1)	−1.7(0.1)	1.3(0.3)	0.5	BO

Table 1. continued

Source name or IRAS name	α_{1950} (h m s)	δ_{1950} (° ′ ″)	Line components	Area (K km s^{-1})	$V_{\rm lsr}$ (km s^{-1})	ΔV (km s^{-1})	$T_{\rm A}^*$ (K)	Source type
EL 1−12	21 45 26.8	47 18 08	1	1.6(0.3)	6.5(0.5)	5.6(0.8)	0.3	BO
			2	1.2(0.2)	4.4(0.1)	1.7(0.2)	0.7	
			1*	0.2(0.1)	4.1(0.1)	1.6(0.2)	0.1	
BD+463471	21 50 39.4	46 59 42	1	0.1(0.1)	5.1(0.8)	3.0(0.1)	0.1	BO
			2	0.3(0.1)	6.6(0.1)	0.8(0.1)	0.4	
S140N	22 17 51.1	63 17 50	1	4.8(0.2)	−8.2(0.1)	2.6(0.1)	1.8	BO
			1*	0.2(0.1)	−8.4(0.1)	1.3(0.3)	0.1	
L1204−A	22 19 50.7	63 36 33	1	2.2(0.5)	−11.2(0.3)	5.3(0.9)	0.4	BO
			2	2.2(0.4)	−10.7(0.1)	1.8(0.2)	1.1	
			1*	0.4(0.1)	−10.7(0.3)	3.3(1.0)	0.1	
L1204−B	22 19 55.7	63 22 12	1	3.4(0.3)	−10.8(0.2)	7.2(0.7)	0.5	BO
			2	1.8(0.3)	−11.0(0.1)	1.9(0.2)	0.9	
			1*	0.4(0.1)	−10.7(0.3)	3.3(1.0)	0.1	
L1221	22 26 37.2	68 45 52	1	1.6(0.1)	−4.3(0.1)	2.2(0.2)	0.7	BO
L1203	22 26 46.7	62 44 22	1	5.1(0.2)	−1.5(0.1)	3.6(0.2)	1.3	BO
			1*	0.2(0.1)	−3.0(0.2)	1.0(0.2)	0.2 d	
			2*	0.2(0.1)	−1.1(0.1)	1.4(0.5)	0.2	
L1206	22 27 12.2	63 58 21	1	0.2(0.1)	−13.3(0.1)	0.8(1.7)	0.2 d	BO
			2	2.4(0.1)	−10.1(0.1)	2.5(0.1)	0.9	
L1251−A	22 34 22.0	75 01 32	1	0.9(0.2)	−3.9(0.4)	5.2(0.9)	0.2	BO
			2	0.5(0.1)	−4.9(0.1)	1.3(0.3)	0.4	
L1251−B	22 37 40.8	74 55 50	1	2.0(0.1)	−3.9(0.1)	2.6(0.1)	0.7	BO
L1211	22 45 23.3	61 46 07	1	2.8(0.2)	−10.6(0.1)	2.6(0.3)	1.0	BO
Cep E	23 01 10.1	61 26 16	1	1.6(0.1)	−11.0(0.1)	2.7(0.1)	0.6	BO
			1*	0.2(0.1)	−11.1(0.2)	1.2(0.4)	0.1	
23032+5937	23 03 16.9	59 37 40	1	5.6(0.4)	−51.2(0.8)	11.1(0.8)	0.5	BO
			2	4.9(0.4)	−51.8(0.8)	3.1(0.8)	1.5	
			1*	0.7(0.2)	−53.1(0.6)	5.9(0.8)	0.1	
			2*	0.5(0.1)	−51.7(0.1)	1.8(0.3)	0.3	
Cep C	23 03 45.6	62 13 49	1	2.0(0.3)	−9.9(0.3)	4.9(0.9)	0.4	BO
			2	1.0(0.3)	−9.7(0.1)	1.3(0.3)	0.7	
NGC 7538S	23 11 36.1	61 10 30	1	5.7(0.2)	−52.1(0.1)	5.7(0.2)	0.9	MMI
			2	30.2(0.2)	−57.0(0.1)	5.3(0.1)	5.4	
			1*	7.9(0.2)	−57.3(0.1)	6.4(0.2)	1.2	
23139+5939	23 13 57.9	59 39 00	1	4.1(0.1)	−45.0(0.1)	3.1(0.1)	1.3	BO
			1*	0.2(0.1)	−44.9(0.1)	1.3(0.3)	0.1	
MWC1080	23 15 14.6	60 34 21	1	2.0(0.1)	−31.1(0.1)	3.5(0.1)	0.5	BO

i.e.
≈ 200 Jy km s^{-1}, "strong". Of 7 strong Class I methanol masers (S235B, G30.80−0.10, W51 e1/e2, W75N, DR21−West, W33−Met, L379IRS3) only one (G30.80−0.10) has a weak CS line (integrated intensity less than 10 K km s^{-1}). The others are stronger.

Class II methanol masers, on average, are more powerful than Class I methanol masers. Twenty-seven Class II methanol masers, detected by Menten (1991), have a flux higher than 100 Jy. It is possible to observe 21 sources of this list at Onsala. Eleven sources were observed in our survey and 6 out of them (S231, S252, G9.62+0.19, W33B, W51, W75 N) exhibit a strong CS line.

All observational data were reduced with the CLASS software package (Groupe d'Astrophysique de Grenoble). The results of the observations are presented in Table 1. Columns 1, 2, and 3 give the source name, R.A. and Dec., respectively; Col. 4 gives the number of components and type of lines (components of the C^{34}S line are marked by a star), and Cols. 5−8 give the Gaussian fitting parameters. In the last column the sources are marked BO – bipolar outflow, MMI – Class I methanol maser, MMII – Class II methanol maser. The list of sources with negative results (emission with $T_{\rm A}^* < 0.03$ K) is presented in Table 2. For the positive results the CS(2−1) line was detected in 93% of the bipolar outflows, in 100% of the Class I methanol masers and in 96% of the Class II methanol masers. All sources observed in the C^{34}S line gave a positive result.

Spectra of sources detected in the CS line only are shown in Fig. i, and spectra of sources detected in both

Table 2. Sources without detected emission in the CS(2−1) line

Source name	α_{1950} (h m s)	δ_{1950} (° ′ ″)	$V_{\rm lsr}$ (km s^{-1})	Source type
LkHα101	04 26 57.2	35 10 01	1.0	BO
ZZ Tau	04 27 50.6	24 35 24	6.2	BO
L1642	04 32 32.0	−14 19 18	10.0	BO
Ori A−E	05 34 11.0	−05 30 03	10.0	BO
G173.59+02.44	05 36 06.4	35 29 21	−13.5	MMII
HD250550	05 59 07.0	16 13 06	2.1	BO
CMa−W	06 56 52.9	−11 54 46	0.0	BO
G22.44−0.18	18 30 01.0	−09 27 00	31.5	MMII
AS353	19 18 08.8	10 56 10	8.0	BO

the CS and C^{34}S lines are shown in Fig. ii (these figures are shown in the online version of the paper only).

A complex line shape was observed in 40% of the sources – one can approximate it as a sum of two Gaussians, a strong narrow and weak broader line. In these cases the parameters of both lines are given in Table 1. The shape of the lines is often asymmetrical and looks like a right or a left wing of the central component.

4. Comments regarding individual sources which have CS(2−1) integrated intensity greater than 10 K km s^{-1}

NGC 281−W. The integrated intensity is 14.4 K km s^{-1}. The profile is based on a pedestal. Bipolar outflow is weak (16 km s^{-1} wing range, Snell et al. 1990). Maser emission at 44 GHz was not detected (Bachiller et al. 1990), but a weak Class II methanol maser was detected at the velocity of the bipolar outflow centre (Slysh et al. 1998).

IRAS05329−0512. The source was taken from the list of bipolar outflows compiled by Xiang & Turner (1995). The coordinates are offset by $\Delta\alpha = 65''$, $\Delta\delta = 40''$ from the centre of the strong Class I methanol maser OMC–2 (Haschick et al. 1990). The CS(2−1) integrated intensity is 11.6 K km s^{-1}. The profile is based on a pedestal.

S233. The integrated intensity is 12.4 K km s^{-1}. The profile is based on a pedestal. IRAS 05358+3543 and a bipolar outflow (CO wing range 25 km s^{-1}, Snell et al. 1990) are observed in the direction of the HII region. The source was observed in CS(2−1) by Bronfman et al. (1996). The velocity of the CS line agrees with the velocity of the bipolar outflow centre within the limits of error. The methanol line at 44 GHz was not detected above the 10 Jy level (Kalenskii et al. 1992).

S231. The integrated intensity is 14.0 K km s^{-1}. The profile is Gaussian. The source is known to be a Class I methanol maser at 44 GHz (Bachiller et al. 1990) and a strong Class II methanol maser at 6.7 GHz (Menten 1991). The velocity of the CS line is −16.5 km s^{-1}.

S235B (GGD 5). A strong CS line with a red-shifted wing was detected. The integrated intensity is 27.4 K km s^{-1}. Bipolar outflow CO wings (22 km s^{-1}) were characterized by Bally & Lada (1983) as being average in range. The velocity of the CS line is −16.9 km s^{-1}. A Class I methanol maser was detected at −16.9 km s^{-1} at 44 GHz at a position with $\Delta\alpha = 12''$ and $\Delta\delta = 23''$ offset (Haschick et al. 1990).

AFGL5180 (S252, G188.9+0.9, S254−258). The region was included in our survey as a bipolar outflow (Snell et al. 1988) and also as a Class II methanol maser (Menten 1991) with $\Delta\alpha = 3''$ and $\Delta\delta = 12''$ position difference. The CS line turned out to be stronger at the position of the bipolar outflow centre than on the position of the methanol maser. The CS integrated intensity is 23.1 K km s^{-1} for AFGL 5180 and 13.8 K km s^{-1} for G188.9+0.9. The velocity of the CS line, 3.2 km s^{-1}, is not coinciding with the velocity of the bipolar outflow 6.7 km s^{-1}, but is coinciding with the velocity 3.15 km s^{-1} of the CS(1−0) line (Anglada et al. 1996) and with the velocity 3.1 km s^{-1} of the CS(2−1) line (Bronfman et al. 1996). Snell et al. (1988) pointed out that it is difficult to evaluate the CO wing range of the bipolar outflow AFGL5180 at the velocity of 4 km s^{-1} due to the second emission component of the line at 8 km s^{-1} from S254−258 star forming region. A strong CS line was observed at 4 km s^{-1} (AFGL 5180 and G188.9+0.9) and a weaker line (16.8 K km s^{-1}) was observed from the HII regions S254−258 at 7.5 km s^{-1}. The latter was observed in the CS(2−1) line by Zinchenko et al. (1994), at a velocity of 7.4 km s^{-1}. A Class II methanol maser was observed at the position of AFGL5180 with the offset $\Delta\alpha = 6''$ and $\Delta\delta = 5''$ (Caswell et al. 1995).

GGD 12−15. The integrated intensity is 11.4 K km s^{-1}. It is a well known bipolar outflow with a wing range of 25 km s^{-1} (Rodríguez et al. 1980; Rodríguez et al. 1982; Harvey et al. 1985; Little et al. 1990). The strong CS line has a main feature and is based on a pedestal. The line velocity, 11.7 km s^{-1}, is coinciding with the velocity of the bipolar outflow (11.6 km s^{-1}) (Rodríguez et al. 1982). No masers were detected, neither at 44 GHz (Bachiller et al. 1990), nor at 6.7 GHz (Slysh et al. 1998).

NGC 2264. The molecular region NGC 2264 has a complex kinematic structure (Crutcher et al. 1978). NGC 2264F and NGC 2264G are two main regions (according to the CO line profile) – the southern and northern parts of the cloud, respectively. NGC 2264(IR) is located in the centre of the cloud and 4′ north of a Bok globule (the Cone Nebula). A methanol maser at 44 GHz was detected by Haschick et al. (1990) at the position of NGC 2264(IR). A thermal methanol emission at 48 GHz was observed at the same position (Slysh et al. 1994) and absorption was observed at 6.7 GHz (Menten 1991). The youngest bipolar outflow (Outflow C.; Margulis & Snell 1988) out of the six observed in this region is close to the position of the observed CS line. The integrated intensity on the position of the IR source is 16.5 K km s^{-1}.

The profile is Gaussian with a small blue-shifted wing.

G9.62+0.19. An intense CS line with a strong pedestal was detected. The integrated intensity is 20.6 K km s^{-1}. There is no information about outflow activity. This is the strongest Class II methanol maser known (Menten 1991; Caswell et al. 1995).

W33−Met. W33 is a giant and well studied HII region (Goldsmith & Mao 1983; Stier et al. 1984). The region contains H_2O and OH masers and far-infrared sources. No Class I methanol maser was detected in W33A and W33B (Haschick et al. 1990), but in both cases strong Class II methanol masers were detected by Menten (1991). Sources of Class I maser emission in W33−Met (Haschick et al. 1990) and a Class II weak maser (Menten 1991) were detected on the periphery of the central radio source W33C (a region of the brightest emission in both IR and CO). The rare methanol maser in the transition $9_{-1} - 8_{-2}$ E at 9.9 GHz was detected in W33−Met, which indicates high-density matter – up to 10^6 cm^{-3} (Slysh et al. 1993). Thermal methanol emission from W33−Met was not studied. From W33A and W33B thermal methanol emission was not detected (Slysh et al. 1994). A strong CS line was detected only at the positions of W33−Met and W33A, the integrated intensity is 41.5 K km s^{-1} for W33−Met, 15.9 K km s^{-1} for W33A, and 3.0 K km s^{-1} for W33B. The velocity of the CS line at the position of both W33−Met and W33A (36 km s^{-1}) is the same as the main velocity of molecular gas, but the CS line from W33B has a velocity of −58 km s^{-1}, which corresponds to another group of gas velocities: the CO spectra of both W33A and W33B contain this group of velocities (Goldsmith & Mao 1983). The CS line profile consists of a single line, but the C^{34}S profile has two features, at 32 km s^{-1} and at 36 km s^{-1}. These correspond to interferometric measurements in this source (Pratap & Menten 1992).

G19.61−0.23. The CS line with integrated intensity 11.8 K km s^{-1} was detected at 42.4 km s^{-1}. The source was included in our list as a Class I methanol maser, which was discovered by Bachiller et al. (1990). Caswell et al. (1995) discovered a weak Class II methanol maser at the position of a weak OH maser with $\Delta\alpha = 9''$ and $\Delta\delta = 42''$ offset ($\sim$ HPBW). They pointed out, however, that the methanol maser was detected with a $39''$ offset from the OH maser position measured with the VLA, which is in agreement with the position of a Class I methanol maser (Forster & Caswell 1989).

L379IRS3. A broad and strong CS line described with a single Gaussian was detected. The integrated intensity is 12 K km s^{-1}. The bipolar outflow has strong wings (48.8 km s^{-1}) (Wilking et al. 1990). A strong Class I methanol maser was detected in this source at 44 GHz (Kalenskii et al. 1992). The velocity of the CS line, 17 km s^{-1}, is 1 km s^{-1} less than the velocity of the maser component (18 km s^{-1}). A Class II methanol maser was discovered in this source in the $15 - 20$ km s^{-1} velocity interval by Caswell et al. (1995) at the position of an OH maser, which was discovered previously.

G34.26+0.16. The profile of the CS line consists of a strong line at 57 km s^{-1} and a weak component. The integrated intensity is 27.0 K km s^{-1}. The region is well studied in different molecules and transitions; this is a very dense region: $n_{H_2} \sim 10^6$ cm^{-3} (Matthews et al. 1987; Fey et al. 1992; Carral & Welch 1992; Heaton et al. 1993). A Class I methanol maser line was detected at 44 GHz (Haschick et al. 1990). A Class II methanol maser was observed also at the position of the strong OH maser and ultracompact HII region in this source (Menten 1991; Caswell et al. 1995). The gas flow is displaced to the blue-shifted side of the spectrum with respect to the molecular cloud, and so is the ultracompact HII region. The ^{12}CO emission line in the (1−0) transition was observed in the $40 - 70$ km s^{-1} velocity interval (Matthews et al. 1987). The cometary nebula G34.26+0.16 is displaced with respect to the molecular cloud and has the velocity 46 km s^{-1} (Fey et al. 1992), but the velocity of the CS line ($\approx$59 km s^{-1}) is the same as for the molecular cloud (Fey et al. 1992). Class I methanol maser emission was observed at 56.4 km s^{-1} and at 58.3 km s^{-1} (Haschick et al. 1990).

W49. This is a well studied region, which has strong bipolar outflow with a wing range of 60 km s^{-1} (Scoville et al. 1986). It was observed in CS by Linke & Goldsmith (1980) at the same velocity (12.1 km s^{-1}), but the spectrum was not published. In our spectrum there is a double line with component velocities of 2.8 km s^{-1} and 12.1 km s^{-1} with integrated intensities 17.3 K km s^{-1} and 5.8 K km s^{-1}, respectively. A weak maser component was observed in methanol at 44 GHz (Haschick et al. 1990) and at 6.7 GHz (Menten 1991).

G45.07+0.13 and G45.47+0.05. These are compact HII regions from the catalogue of OH masers (Caswell & Haynes 1983). The CS line integrated intensities are 12.7 K km s^{-1} and 10.4 K km s^{-1}, respectively. There is a small asymmetry in the line profile. A weak Class II methanol maser was observed (Menten 1991).

W51. This is a well studied region of star formation (Turner et al. 1973; Liszt & Linke 1975; Linke & Goldsmith 1980; Pratap & Menten 1992). The parameters of the CS line, which were obtained previously, are in good agreement with the present results. It is a well known Class I and Class II source of maser emission (Haschick et al. 1990; Menten 1991). The CS line was observed at the position of both the Class II methanol maser W51 and the Class I methanol maser W51 e1/e2, which are very close. The CS line is stronger at the position of the Class I methanol maser, 114.7 K km s^{-1} (72.4 K km s^{-1} at the position of the Class II methanol maser). The velocities of the lines differ by 2 km s^{-1}.

ON1. The integrated intensity is 11.1 K km s^{-1}. This is an isolated ultracompact HII region; the region of the first generation of star formation; one of the smallest in

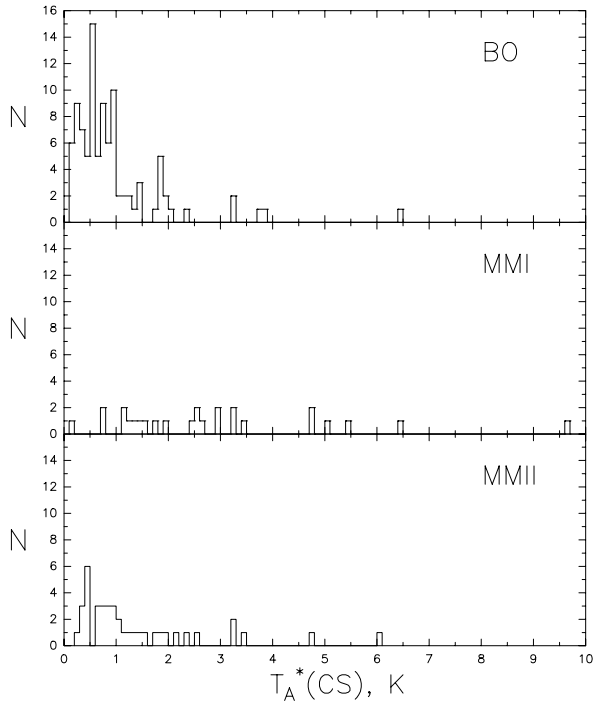

Fig. 1. Distributions of the CS(2−1) line intensities of bipolar outflows (BO), of Class I (MMI), and of Class II (MMII) methanol masers

the Galaxy (approx. 0.02 pc) and one of the youngest (approx. 2000 years); the densest part of the molecular cloud has the density $n_{H_2} > 10^4 - 10^5$ cm^{-3}; the region contains OH and H_2O masers; there is a bipolar outflow with a wing range of up to 30 km s^{-1} (Israel & Wooten 1983; Zheng et al. 1985). The velocity of the main component of the CS profile, 11 km s^{-1}, is coinciding with the velocities of CO lines, of NH_3 lines, and of the group of OH masers. The velocity of the pedestal coincides with that of the H76α recombination line, 5.1 km s^{-1} (Zheng et al. 1985). This is a source of Class I and Class II methanol maser emission; at 44 GHz the velocity is also approximately 11 km s^{-1} (Haschick et al. 1990; Menten 1991).

ON2. There are two peaks of CO emission – central and north (Matthews et al. 1986). Bachiller et al. (1990) discovered a Class I methanol maser close to the position of the peak of CO emission and OH maser emission with $\Delta\delta = -36''$ offset. Menten (1991) discovered a Class II methanol maser at 6.7 GHz at the position of the Class I methanol maser. Thermal methanol emission was discovered at 48 GHz (Slysh et al. 1994). In our survey a strong CS line with an integrated intensity of 21.4 K km s^{-1} was detected. The CO spectrum consists of three peaks at the position of the methanol maser. The CS profile has one component. No strong bipolar outflow has been detected (Matthews et al. 1986), but CO lines have wings at both the red and the blue-shifted side with a range of up to 30 km s^{-1}.

DR21−West, DR21−Met C, W75N. This is a well known and well studied region in CS (Turner et al. 1973; Liszt & Linke 1975; Linke & Goldsmith 1980; Haschick et al. 1981; Plambeck & Menten 1990). The CO line from DR21 (bipolar outflow) was observed at the velocity of −3.0 km s^{-1} and from W75N at −9 km s^{-1}. The red wing range of the CO line in DR21 is difficult to estimate due to the influence of the blue-shifted wing from W75N (Fisher et al. 1985). CS line parameters in our survey for DR21−West and DR21−Met C correspond to line parameters of the previous observations (Linke & Goldsmith 1980; Plambeck & Menten 1990). DR21−West, DR21−Met C, and W75N are the strongest Class I methanol masers (Haschick et al. 1990) and at the same time W75N is one of the strongest Class II methanol masers (Menten 1991). Integrated intensities of DR21−West, DR21−Met C, and W75N are 17.2 K km s^{-1}, 25.9 K km s^{-1}, and 22.7 K km s^{-1}, respectively.

IRAS23032+5937. The integrated intensity is 10.5 K km s^{-1}. The CS line velocity corresponds to the velocity of the Perseus arm. The bipolar outflow has wings with a small range of 20 km s^{-1} (Wouterloot et al. 1989).

NGC 7538S. This is the southern part of a well known star forming region. There is no bipolar outflow (Fukui 1989). Haschick et al. (1990) discovered a group of methanol masers at this position. Emission lines are merged into a wide component at 44 GHz. The strong CS line profile is a simple Gaussian with a small asymmetry in the right wing. The CS integrated intensity is 35.9 K km s^{-1}.

5. Discussion of the results

5.1. Intensities and line widths

Figure 1 shows the distribution of the CS(2−1) line intensities of bipolar outflows and of Class I and Class II methanol masers. The distributions of the intensities are approximately the same for bipolar outflows and for Class II methanol masers: $\overline{T}_A^* = 0.95 \pm 0.09$ K and $\overline{T}_A^* = 1.38 \pm 0.22$ K, respectively. The Class I methanol masers are stronger in CS: $\overline{T}_A^* = 2.86 \pm 0.41$ K.

Figure 2 shows the distributions of the CS(2−1) line widths (main feature) for bipolar outflows and for Class I and Class II methanol masers. Methanol masers have, in general, wider main features:

$\Delta V_{\rm main}$(CS)(BO) = (2.33 ± 0.15) km s^{-1}
$\Delta V_{\rm main}$(CS)(MMI) = (6.21 ± 0.55) km s^{-1}
$\Delta V_{\rm main}$(CS)(MMII) = (4.80 ± 0.34) km s^{-1}.

Figure 3 shows the distributions of the CS(2−1) widths of wings for bipolar outflows and for Class I and II methanol

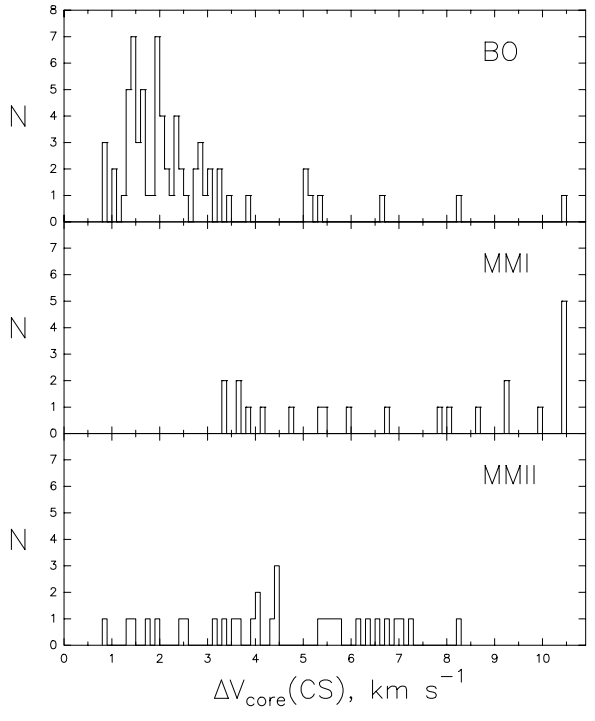

Fig. 2. Distributions of the CS(2−1) line widths (main feature) for bipolar outflows (BO), for Class I (MMI), and for Class II (MMII) methanol masers

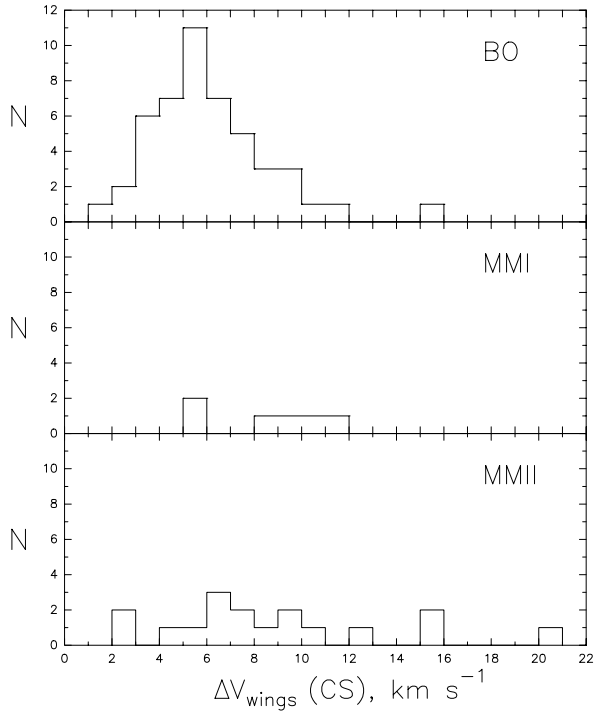

Fig. 3. Distributions of the CS(2−1) widths of wings for bipolar outflows (BO), for Class I (MMI), and for Class II (MMII) methanol masers

masers. A complex line shape was observed in 52% of the bipolar outflows, in 23% of the Class I methanol masers, and in 37% of the Class II methanol masers. We adopted as the wing of a CS line the HPBW of the pedestal. The wings of the CS lines have a negligible range:
$\Delta V_{\rm wings}$(CS)(BO) = (6.15 ± 0.38) km s^{-1}
$\Delta V_{\rm wings}$(CS)(MMI) = (8.37 ± 0.97) km s^{-1}
$\Delta V_{\rm wings}$(CS)(MMII) = (8.71 ± 1.28) km s^{-1}.
Thus, the results of our observations confirm the conclusion of Thronson & Lada (1984), that wide wings in CS are rare.

5.2. Column densities

An evaluation of the CS column density for an optically thin layer was done with the formula taken from Knee et al. (1990).

The results of the observations of the CS(2−1) line and of the isotopic C^{34}S(2−1) line allow us to calculate the value of the optical depth in CS (e.g. Zinchenko et al. 1994).

The resulting column density value should be defined more precisely in conformity with the equation:

$$N' = \frac{\tau}{1 - {\rm e}^{-\tau}} N, \qquad (1)$$

where τ is the optical depth and N is the CS column density for an optically thin layer. The results of the calculations are given in Table 3. First column – source name, second – optical depth for sources which were observed in both CS and C^{34}S, third – CS column density (optical depth was taken into consideration).

Figure 4 shows the distributions of the CS column density for bipolar outflows and for Class I and Class II methanol masers.

The average values $\overline{N}_{\rm CS}$ are the following:
$\overline{N}_{\rm CS}$(BO) = (2.0 ± 0.6) 10^{14} cm^{-2}
$\overline{N}_{\rm CS}$(MMI) = (9.8 ± 0.9) 10^{14} cm^{-2},
$\overline{N}_{\rm CS}$(MMII) = (11.9 ± 1.2) 10^{14} cm^{-2}.
These estimates of the centres of bipolar outflows are in good agreement with others: for example, in one of the first surveys of molecular clouds, which was carried out by Liszt & Linke (1975). The typical value of the CS(2−1) concentration is 10^{14} cm^{-2}, but in methanol masers this value is an order of magnitude higher.

Errors of the average values are given as:

$$\sigma = \sqrt{\frac{\sum (\bar{x} - x_i)^2}{n(n-1)}} \qquad (2)$$

where $\bar{x}$ is the average value, x_i is an individual value and n is the number of values.

Table 3. Column density of BO and MM

Source name	Optical depth	N_{CS} (10^{14}cm^{-2})
NGC 281−W	2.99	3.79
IC1805−W	3.59	0.71
L1455 (RNO15FIR)	3.31	1.02
05329−0512	1.57	0.95
L1641−N	0.99	0.36
S233	3.31	1.84
S231	2.43	3.41
S235B (GGD 5)	0.38	0.48
AFGL5180	1.96	2.40
GGD 12−15	5.68	3.18
S254−258	3.40	3.43
S255	4.79	1.94
NGC 2264(IR)	4.53	5.43
W33−Met	3.71	16.4
W33A	23.8	24.9
G19.61−0.23	8.23	10.6
W42	9.52	5.68
G30.80−0.10	4.00	1.31
18497+0022	19.5	4.68
G34.26+0.16	2.33	7.41
G35.03+0.35	19.7	5.19
G35.05−0.52	9.86	2.80
W48	13.7	12.5
G40.62−0.14	9.18	5.32
W49	6.20	11.7
G43.80−0.13	22.3	10.9
G45.07+0.13	3.60	2.49
G45.47+0.05	5.07	4.62
W51M	8.04	8.38
W51−Met1	1.93	5.48
W51 e1/e2	1.31	11.9
W51−Met2	4.93	13.7
W51−Met4	3.76	5.69
W51−Met5	1.17	3.50
ON1	4.70	4.73
20126+4104	5.21	1.32
ON2	34.4	80.4
W75N	2.14	3.45
DR21−West	5.62	3.57
DR21−Met C	1.51	1.59
V645Cyg	6.41	1.32
EL 1−12	4.36	0.56
S140N	0.50	0.16
L1204−A	1.38	0.26
L1204−B	2.23	0.39
L1203	2.14	1.06
Cep E	5.73	0.97
23032+5937	3.88	2.01
NGC 7538S	5.13	16.8
23139+5939	2.08	0.83

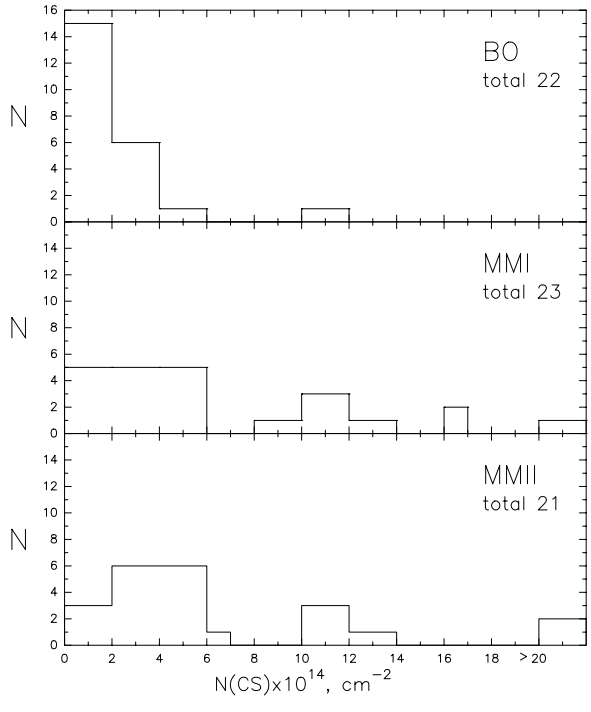

Fig. 4. Distributions of the CS column density for bipolar outflows, for Class I, and for Class II methanol masers

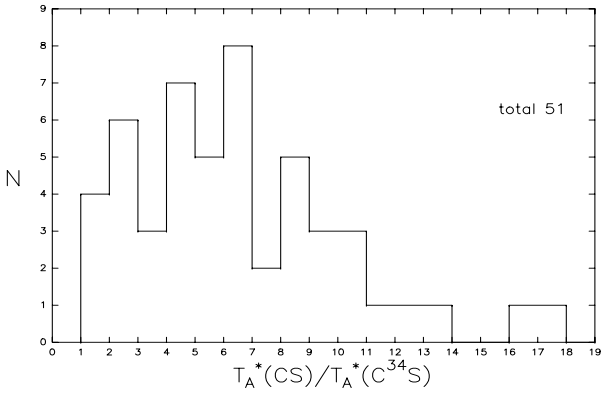

Fig. 5. Distribution of the $T_A^*(CS)/T_A^*(C^{34}S)$ ratio for 51 sources observed in the $C^{34}S$ line

Figure 5 shows the distribution of the $T_A^*(CS)/T_A^*(C^{34}S)$ ratio for the 51 sources observed in the $C^{34}S$ line. This distribution lies below the terrestrial value of 22.5 and for most of the sources the ratio is below 10. We conclude, therefore, that all our sources are optically thick.

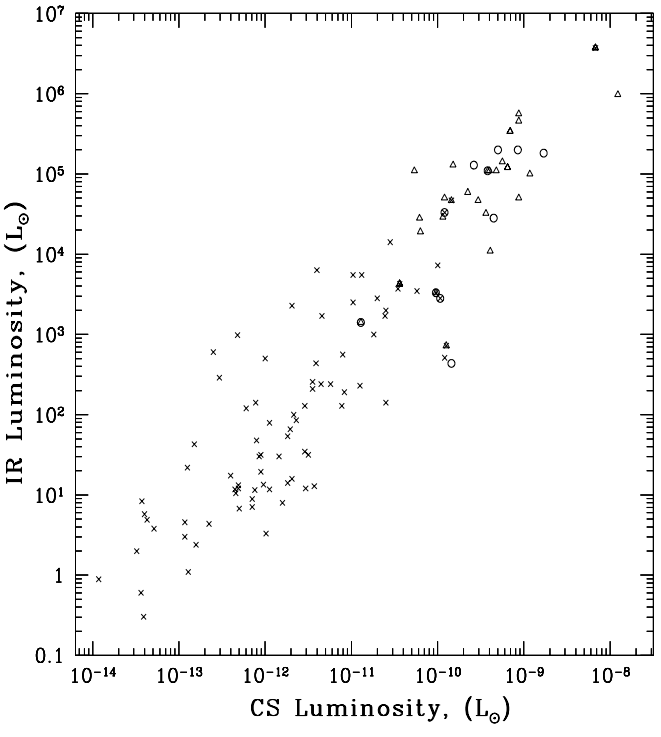

Fig. 6. Dependence between the IR and the CS luminosity for bipolar outflows (crosses), for Class I (circles), and for Class II (triangles) methanol masers

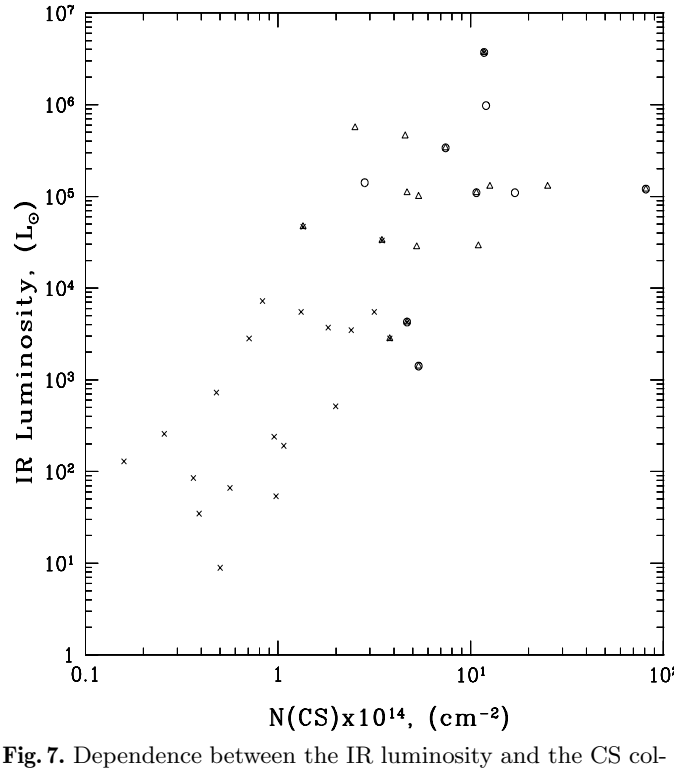

Fig. 7. Dependence between the IR luminosity and the CS column density for bipolar outflows (crosses), for Class I (circles), and for Class II (triangles) methanol masers

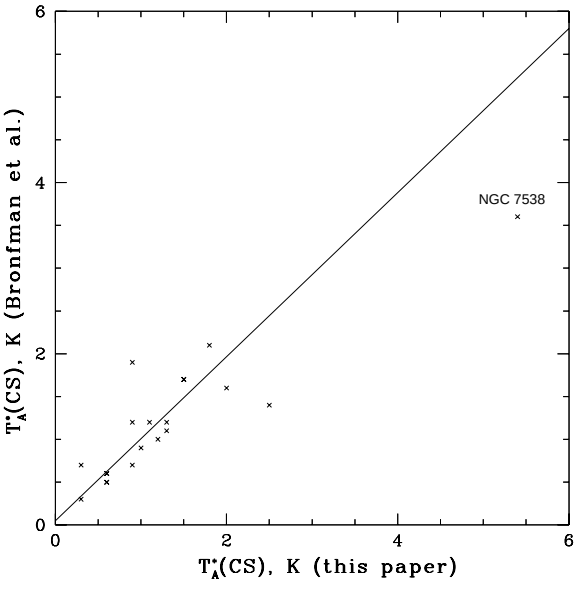

Fig. 8. Distributions of the antenna temperature in CS(2−1) line of our survey – x-axis and Bronfman et al. (1996) survey in CS(2−1) line – y-axis for bipolar outflows and for Class I and Class II methanol masers. The straight line is the best linear fit to the data

5.3. IR luminosity of the sources

The infrared data of the sources as measured by IRAS are presented in Table 4. The columns list the IRAS source name, the IRAS identification, the IRAS flux densities, the distance, partially taken from other papers, partially calculated with the help of the Brand & Blitz (1994) Galactic rotation curve, and IR luminosity L calculated from the Morgan & Ballyformula (1991):

$$L(L_\odot) = 23.0\left(\frac{D}{500\ \mathrm{pc}}\right)^2 \int \frac{S}{\lambda^2}\mathrm{d}\lambda\,, \qquad (3)$$

where S is the IRAS flux density in Jy, D is the distance to the source in units of 500 pc, and λ is the wavelength in μm. The integral is calculated as the sum of the 4 areas bounded by the IRAS wavelengths (12, 25, 60, and 100 μm) and by straight lines connecting the flux densities. No extrapolation is done to wavelengths below 12 and above 100 μm. References from where the distances were taken are presented in the last column of Table 4. The sizes of the CS regions are unknown. We have calculated the CS luminosity using the distances listed in Table 4 and the integrated intensities assuming that all sources are "point sources" for the beam of the Onsala radio telescope. Figure 6 shows the dependence between the IR luminosity and the CS luminosity for bipolar outflows (crosses) and for Class I (circles) and Class II (triangles) methanol masers. One can see that the bipolar outflows are primarily located in the region of low intensity both in

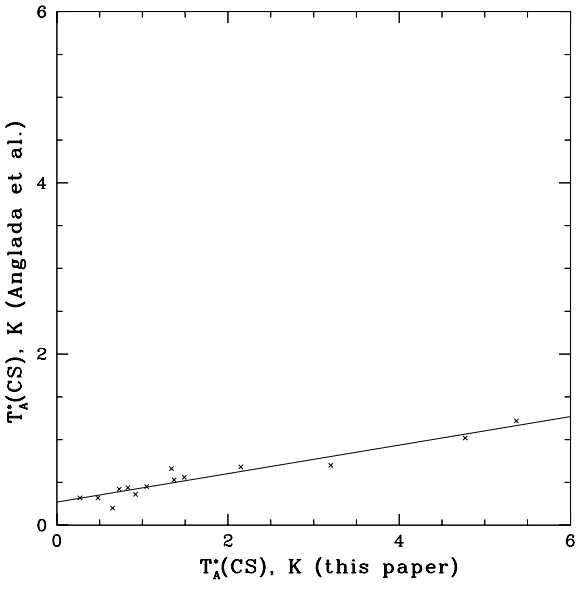

Fig. 9. Distributions of the antenna temperature in CS(2−1) line of our survey − x-axis and Anglada et al. (1996) in CS(1−0) line − y-axis for bipolar outflows and for Class I and Class II methanol masers. The straight line is the best linear fit to the data

CS and in the IR. On the contrary, Class I and II methanol masers are stronger both in CS and in the IR.

The 51 brightest sources in the CS line were observed in the $C^{34}S$ line. Of these 51 sources, 37 were associated with IRAS sources. Figure 7 shows the dependence between the IR luminosity and the CS column density for bipolar outflows (crosses) and for Class I (circles) and Class II (triangles) methanol masers. The dependence shows that low luminosity IRAS objects are mainly associated with low column density and that high luminosity IRAS objects are associated with high column density.

From Figs. 6 and 7 we conclude that methanol masers are formed in denser regions than bipolar outflows. Besides, Figs. 6 and 7 indicate that distance estimates and IRAS identifications are relatively correct.

6. Comparison with other surveys

Figure 8 shows the antenna temperature of the CS(2−1) line in the survey of Bronfman et al. (1996) plotted against the same quantity in our survey. The survey of Bronfman et al. was carried out also using the 20-m Onsala radio telescope. The straight line is the least-squares linear fit to the data. Its equation is:

y=(0.91 ± 0.16)x+(0.16 ± 0.19)

and the correlation coefficient is $r = 0.85$. Since both data sets have been obtained from the same line using the same instrument, ideally the slope should be unity and the offset at $x = 0$ should be zero. The statistical errors of these two quantities (1σ) are such that they allow these ideal values. The dispersion of the measured values from the fitted line is consistent with a calibration uncertainty of typically $20 - 30\%$. This is expected for an observing site at sea level such as Onsala.

Figure 9 shows the antenna temperature of the CS(1−0) line in the survey of Anglada et al. (1996) plotted against the antenna temperature of the CS(2−1) line in our survey. The survey of Anglada et al. was carried out using the 37-m radio telescope at the Haystack Observatory. The HPBW of this telescope is $41''$ at the CS(1−0) frequency, i.e. similar to the HPBW of the Onsala telescope at twice the frequency. The least-squares fit to the data is described by:

y=(0.17 ± 0.02)x+(0.27 ± 0.12)

and the correlation coefficient is $r = 0.95$. Since both the (2−1) and the (1−0) lines are optically thick, the ratio between the antenna temperatures in Anglada's survey and in ours could be explained by the ratio between the beam efficiencies of the Haystack telescope (9%) and of the Onsala telescope (56%): 0.16.

There seems to be a systematic offset between the antenna temperatures measured by Anglada et al. and our values by ~ 0.3 K. The reason for this is unclear. However, the statistical significance of this offset is poor ($\sim 2\sigma$).

7. Conclusions

1. Observations of 158 sources in the CS(2−1) line have been carried out (111 bipolar outflows, 26 Class I methanol masers, and 47 Class II methanol masers, 10 sources are Class I and Class II methanol masers simultaneously), with 149 positive results (97 bipolar outflows, 26 Class I methanol masers, and 45 Class II methanol masers). Out of these 149 sources, 51 have been observed in $C^{34}S$. All sources observed in the $C^{34}S$ line show positive results.
2. The main feature of the CS line for Class I methanol masers, is on average, wider than for bipolar outflows and Class II methanol masers.
3. A complex line shape was observed in 52% of bipolar outflows, in 23% of Class I methanol masers, and in 37% of Class II methanol masers. Considering the pedestal of a line as wings, one can see that the range of the wings of the CS lines is insignificant.
4. The column density in methanol masers, both of Class I and Class II, is higher than in bipolar outflow centres.
5. Assuming that all sources are "point sources" for the beam of the Onsala radio telescope, we conclude that the dependence between the CS luminosity and the IR luminosity has been proven. Methanol masers, both of Class I and Class II, are stronger than bipolar outflows both in the IR continuum and in the CS line. Methanol masers of both classes are formed in denser regions than bipolar outflows.

Table 4. IRAS data

Source name	IRAS identification	$S12$ (Jy)	$S25$ (Jy)	$S60$ (Jy)	$S100$ (Jy)	Distance (kpc)	Luminosity ($L_\odot$)	Reference
LkH$_\alpha$198	00087+5833	33	88.1	127.2	182.8	1	5 10^2	Fukui (1989)
00213+6530	00213+6530	0.3	1	4.9	15	0.85	8	Fukui (1989)
00259+6510	00259+6510	0.75	1.9	7.8	32.6	0.85	16	Fukui (1989)
L1293	00379+6248	0.3	0.4	9.9	27	0.85	13	Fukui (1989)
NGC 281−W	00494+5617	1.8	13.4	329.6	1166	2.1	2.8 10^3	Fukui (1989)
NGC 281−E	00512+5617	2	10.8	44.8	218.2	2.1	5.6 10^2	Fukui (1989)
S187−IRS	01202+6133	10	180	880	1700	2.0	6.3 10^3	Fukui (1989)
IC1805−W	02252+6120	9.8	56	239.5	638.8	2.3	2.8 10^3	Fukui (1989)
RNO13	03220+3035	9	2.8	4	9.86	0.2	2.0	Fukui (1989)
RNO15FIR	03245+3002	0.3	3.4	47.1	93.6	0.35	9.0	Fukui (1989)
03262+3108	03262+3108	0.4	0.9	0.4	947.1	0.28	21.8	this paper
T Tau	04190+1924	15	44	99	98	0.14	4.9	Fukui (1989)
04191+1523	04191+1523	0.3	1.3	5.9	14.4	0.14	0.3	Fukui (1989)
HARO 6−10	04263+2426	14.9	38.9	59.7	47.3	0.14	3.8	Fukui (1989)
IC2087	04369+2539	5	6.8	7.3	18.2	0.14	0.9	Fukui (1989)
L1634	05173−0555	0.3	3	27.1	61.3	0.5	11.6	Fukui (1989)
Ori A−W	05302−0537	4.3	19.3	55.3	82.4	0.5	30.2	Fukui (1989)
05329−0512	05329−0512	22.8	54.2	630.7	22.7	0.58	2.4 10^2	this paper
L1641−N	05338−0624	0.5	16.4	206.3	487.7	0.5	85.5	Fukui (1989)
NGC 1999	05339−0644	8.6	8.9	75.9	38.6	0.5	31.8	Fukui (1989)
AFGL 5157	05345+3157	12.3	18.9	339	565	1.8	1.7 10^3	Fukui (1989)
Ori I−2	05355−0146	0.39	1.4	13.3	42.1	0.4	4.4	Fukui (1989)
S233	05358+3543	5.6	74.7	722.3	1310	1.8	3.7 10^3	Fukui (1989)
L1641−C	05363−0702	0.53	4.8	23.6	59.3	0.5	11.8	Fukui (1989)
GGD 4	05373+2349	9	26.6	125.2	193.8	1.0	2.4 10^2	Fukui (1989)
S235B	05375−0731	0.3	8.8	157.1	271.7	1.8	7.3 10^2	Fukui (1989)
L1641−S3	05375+3540	28.3	226.4	1709	1635	0.5	6.0 10^2	Fukui (1989)
L1641−S	05380−0728	28.2	89.6	186.9	227.3	0.5	1.2 10^2	Fukui (1989)
L1641−S4	05384−0808	0.4	0.9	16.1	40.2	0.5	7.1	Fukui (1989)
L1641−S2	05403−0818	0.9	4.2	14	16.6	0.5	6.8	Fukui (1989)
HH26IR	05435−0015	1.9	5.1	20.9	67.9	0.5	13.5	Fukui (1989)
HH24	05435−0011	2.1	9.2	27.6	30.8	0.5	14.1	Fukui (1989)
NGC 2068 H_2O	05437−0001	8.1	23.9	229.3	507.4	0.5	1.0 10^2	Fukui (1989)
S242	05490+2658	6.5	30.1	340.4	681.9	2.1	2.5 10^3	Fukui (1989)
L1617	05491+0247	0.3	6.7	43.9	72.1	0.5	17.4	Fukui (1989)
L1598−NW	05494+0820	0.3	0.7	8.7	16.4	0.9	11.7	Fukui (1989)
L1598	05496+0812	0.4	3.3	22	39.8	0.9	30.0	Fukui (1989)
AFGL5180	06058+2138	14	140.2	955.5	1666	1.5	3.5 10^3	Fukui (1989)
GGD 12−15	06084−0611	27.1	603.5	3613	4876	1.0	5.5 10^3	Fukui (1989)
S254−258	06099+1800	107.2	371.6	3145	5285	2.5	3.3 10^4	Fukui (1989)
Mon R2−E	06103−0612	4	20.8	70.3	122.8	0.95	1.3 10^2	Fukui (1989)
RNO 73	06308+0402	13.4	38.3	602	949	1.6	2.3 10^3	Fukui (1989)
R Mon	06364+0846	54.7	132	121	149	0.7	2.9 10^2	Fukui (1989)
Mon OB1−D	06382+0939	7.1	16.3	212.8	499.3	0.76	2.1 10^2	Fukui (1989)
Mon OB1−G	06384+0958	0.3	0.29	6.4	32	0.76	10.5	Fukui (1989)
NGC 2264−G	06384+0932	145.5	324.9	910.8	1560	0.76	1.4 10^3	Fukui (1989)
S287−N	06453−0209	1.1	6.1	22.2	36.9	2.3	2.3 10^2	Fukui (1989)
BFS 56	06567−0350	4.7	14.5	56.5	779.6	2.3	1.7 10^3	Fukui (1989)
L1654	06572−0742	18.2	141	419	474	1.1	9.7 10^2	Fukui (1989)
G9.62+0.19	18032−2032	38.6	292.4	4106	7844	5.7	2.0 10^5	Cesaroni et al. (1994)
W33B	18106−1802	3.2	5.2	132.6	427.2	4.9	4.4 10^2	Stier et al. (1984)
W33A	18117−1753	21.1	269	2228	6310	3.7	1.3 10^5	Stier et al. (1984)
18128−1640	18128−1640	15.6	37.2	471	1017	15	1.8 10^5	this paper
L483	18148−0440	0.25	6.9	89	166	0.25	8.4	Fukui (1989)
G18.46−0.01	18217−1252	2.9	41	850.3	1886	12.1	2.0 10^5	this paper
G19.61−0.23	18248−1158	47.8	406.9	4635	7093	4	1.1 10^5	Genzel & Downes (1977)

Table 4. continued

Source name	IRAS identification	$S12$ (Jy)	$S25$ (Jy)	$S60$ (Jy)	$S100$ (Jy)	Distance (kpc)	Luminosity ($L_\odot$)	Reference
G20.24+0.08	18249−1116	3.43	6	116	370	11.1	2.8 10^4	this paper
L379IRS3	18265−1517	1.5	46.5	445.2	1297	2	3.3 10^3	Schwartz et al. (1988)
L379IRS2	18277−1516	3.6	2.1	147.1	388.4	2	1.0 10^3	Schwartz et al. (1988)
G24.33+0.11	18328−0738	12.5	7.5	20	201	8.88	1.1 10^4	this paper
18379−0500	18379−0500	27.9	54.2	748	1278	7.8	5 10^4	Waller et al. (1987)
G28.83−0.25	18421−0348	5.6	60.8	713	1877	6.3	5.0 10^4	Solomon et al. (1987)
G30.82+0.28	18440−0148	2.1	31	334	1224	8.22	4.7 10^4	this paper
W43M	18456−0129	4.9	89	1071	3693	7.3	1.1 10^5	Kuchar & Bania (1994)
G33.13−0.09	18496+0004	3.2	24.1	591.4	2179	7.1	5.9 10^4	Kuchar & Bania (1994)
18497+0022	18497+0022	13.4	31.2	546	2064	9.5	1.1 10^5	Kuchar & Bania (1994)
G34.26+0.16	18507+0110	140.2	1106	11500	32460	3.8	3.4 10^5	Fey et al. (1992)
G35.03+0.35	18515+0157	5.4	42.2	1333	3297	3.6	2.8 10^4	Anglada et al. (1996)
G35.05−0.52	18545+0134	14.2	77.7	772.2	1487	10.4	1.4 10^5	this paper
18572+0057	18572+0057	2.4	11.3	151	414.2	10.7	3.2 10^4	Fukui (1989)
W48	18592+0108	114.5	1023	10150	13960	3.0	1.3 10^5	this paper
G40.62−0.14	19035+0641	2.3	66.7	610.3	922.7	10.5	9.9 10^4	Kuchar & Bania (1994)
W49	19078+0901	105.3	1090	7566	36150	14	3.7 10^6	Braz & Epchtein (1983)
G43.80−0.13	19095+0930	5.3	129.1	1725	2744	3.43	2.9 10^4	Fukui (1989)
G45.07+0.13	19110+1045	57.6	494.3	5913	7497	8.3	5.6 10^5	this paper
G45.47+0.13	19117+1107	37.3	303.5	2608	7890	9.5	4.6 10^5	Fukui (1989)
L673	19180+1116	1.1	2.2	3.5	87	0.3	3.3	this paper
W51 e1/e2	19213+1424	424.2	4344	4.8	26760	7.6	9.7 10^5	Israel & Wotten (1983)
L810	19433+2743	1.1	4.9	30.1	84	1.5	1.4 10^2	Fukui (1989)
19589+3320	19589+3320	3.2	20.1	156.3	420.9	7.97	1.9 10^4	Anglada et al. (1996)
ON1	20081+3122	1.1	58.8	1431	3119	1.4	4.3 10^3	Fukui (1989)
20126+4104	20126+4104	2.5	108.9	1382	1947	1.7	5.5 10^3	Fukui (1989)
ON2	20198+3716	73.8	480.5	5446	6985	3.9	1.2 10^5	Fukui (1989)
AFGL2591	20275+4001	438.9	1112	5314	5721	1.2	1.4 10^4	Fukui (1989)
L1036	20377+5658	0.77	2	5.8	13	0.44	3.0	Fukui (1989)
L1157	20386+6751	0.3	0.3	10.9	43.5	0.44	4.6	Fukui (1989)
PVCep	20453+6746	12.8	33	49	58	0.5	42.2	Fukui (1989)
L1228	20582+7724	1.2	3.2	11.8	18.1	0.15	0.6	Fukui (1989)
V1331Cyg	20595+5009	1.2	2.8	6.6	39.8	0.7	13.2	Fukui (1989)
L988−a	21007+4951	0.9	5.1	21.8	31.6	0.7	19.4	Fukui (1989)
L988−e	21023+5002	24	34	87	199	0.7	1.4 10^2	Fukui (1989)
IC1396W	21246+5743	0.3	0.6	9.7	38.3	0.75	12.0	Fukui (1989)
V645 Cyg	21381+5000	114.2	219.3	370.5	454.6	6	4.7 10^4	Fukui (1989)
IC1396E	21445+5712	3	11.3	34.8	86.8	0.75	48.4	Fukui (1989)
EL 1−12	21454+4718	2.4	8	40	83.5	0.9	65.8	Fukui (1989)
BD463471	21506+4659	1.6	1.7	2.6	9.5	0.9	12.0	Fukui (1989)
S140N	22178+6317	5.15	14.4	61.6	212	0.9	1.3 10^2	Fukui (1989)
L1204−A	22198+6336	0.25	23.3	187	414	0.9	2.6 10^2	Fukui (1989)
L1204−B	22199+6322	0.79	3.82	20.2	55.2	0.9	34.5	Fukui (1989)
L1221	22266+6845	0.98	3.54	12.3	25.9	0.2	1.1	Fukui (1989)
L1203	22267+6244	1.92	11.9	152	287	0.9	1.9 10^2	Fukui (1989)
L1206	22272+6358	2.58	1.94	378	726	0.9	4.4 10^2	Fukui (1989)
L1251−A	22343+7501	5	26	66	80	0.2	5.7	Fukui (1989)
L1251−B	22376+7455	0.8	5.6	32	67	0.2	2.4	Fukui (1989)
L1211	22453+6146	2.71	5.65	19.7	63.6	0.75	31.6	Fukui (1989)
Cep E	23011+6126	0.43	5.77	60.9	112	0.75	53.1	Fukui (1989)
23032+5937	23032+5937	0.25	1.68	26.3	55.9	3.5	5.1 10^2	Fukui (1989)
Cep C	23037+6123	2.49	4.32	80.7	197	0.75	80.1	Fukui (1989)
NGC 7538S	23116+6111	243	1781	7073	14140	2.8	1.1 10^5	Fukui (1989)
23139+5939	23139+5939	2.9	50.1	366	685	3.5	7.3 10^3	Fukui (1989)
MWC1080	23152+6034	22.2	25.07	147	227	2.5	2.0 10^3	Fukui (1989)

6. The statistical characteristics of the regions forming Class I methanol masers are different from those both in the centres of bipolar outflows and in the regions forming Class II methanol masers, based on the values of the average antenna temperature, average column density, and IR luminosities in the CS(2−1) line. It is possible that physical conditions in bipolar outflows are closer to physical conditions of Class II methanol masers.

Acknowledgements. We are grateful to V.I. Slysh, S.V. Kalenskii, A.M. Dzura, and M.A. Voronkov for critically reading the manuscript, G.M.L, I.E.V. & V.V.G. are grateful also to R. Hammargren for the excellent professional skill during the time of our observations. This work (G.M.L., I.E.V. & V.V.G.) was supported by the Russian Foundation for Basic Research (grant No. 95−02−05826). The observations were carried out during the stay of G.M.L. and I.E.V. at the Onsala Space Observatory with support from the Swedish Royal Academy of Sciences. The Onsala Space Observatory is the Swedish National Facility for Radio Astronomy and is operated by Chalmers University of Technology, Göteborg, Sweden, with financial support from the Swedish Natural Science Research Council and the Swedish Board for Technical Development.

References

Anglada G., Estalella R., Pastor J., Rodríguez L.F., Haschick A.D., 1996, ApJ 463, 205
Bachiller R., Cernicharo J., Martín−Pintado J., Tafalla M., Lazareff B., 1990, A&A 231, 174
Bachiller R., Gómez−González J., 1992, A&AR 3, 257
Bachiller R., Liechti S., Walmsley C.M., Colomer F., 1995, A&A 295, L51
Bally J., 1982, ApJ 261, 558
Bally J., Lada C.J., 1983, ApJ 265, 824
Bally J., Lane A.P., 1991, in: The Physics of Star Formation and Early Stellar Evolution, Lada and Kylafis (eds.). Kluwer Academic Publishers, Dordrecht, p. 471
Batrla W., Matthews H.E., Menten K.M., Walmsley C.M., 1987, Nat 326, 49
Bronfman L.−Å., Nyman L.−Å., May J., 1996, A&AS 115, 81
Brand J., Blitz L., 1994, A&A 275, 67
Braz A., Epchtein N., 1983, A&AS 54, 167
Carral P., Welch W.J., 1992, ApJ 385, 244
Caswell J.L., Haynes R.F., 1983, Aust. J. Phys. 36, 417
Caswell J.L., Vaile R.A., Ellingsen S.P., Whiteoak J.B., Norris R.P., 1995, MNRAS 272, 96
Churchwell E., Walmsley C.M., Wood D.O.C., 1992, A&A 253, 541
Cesaroni R., Churchwell E., Hofner P., Walmsley C.M., Kurtz S., 1994, A&A 288, 903
Crutcher R.M., Hartkopf W.I., Giguerre P.T., 1978, ApJ 226, 839
Fey A.L., Claussen M.J., Gaume R.A., Nedoluha G.E., Johnston K.J., 1992, AJ 103, 234
Fisher J., Sanders D.B., Simon M., Solomon P.M., 1985, ApJ 293, 508
Forster J.R., Caswell J.L., 1989, A&A 213, 339
Fukui Y., 1989, in: Low Mass Star Formation and Pre−Main Sequence Objects, Reipurth (ed.). ESO, Garching bei München, p. 95
Genzel R., Downes D., 1977, A&AS 30, 145
Goldsmith P.F., Mao X.−J., 1983, ApJ 265, 791
Haschick A.D., Reid M.J., Burke B.F., Moran J.M., Miller G., 1981, ApJ 244, 76
Haschick A.D., Menten K.M., Baan W.A., 1990, ApJ 354, 556
Harvey P.M., Wilking B.A., Joy M., Lester D.F., 1985, ApJ 288, 725
Heaton B.D., Little L.T., Yamashita T., et al., 1993, ApJ 278, 238
Israel F.P., Wootten H.H., 1983, ApJ 266, 580
Johnston K.J., Gaume R., Stolovy S., Wilson T.L., Walmsley C.M., Menten K.M., 1992, ApJ 385, 232
Juvela M., 1996, A&AS 118, 191
Kalenskii S.V., Bachiller R., Berulis I.I., et al., 1992, AZh 69, 1002
Kalenskii S.V., Berulis I.I., Val'tts I.E., Dzura A.M., Slysh V.I., Vasil'kov V.I., 1994, AZh 71, 51
Knee L.B.G., Cameron M., Liseau R., 1990, A&A 231, 419
Kuchar T.A., Bania T.M., 1994, ApJ 436, 117
Kutner M.L., Ulich B.L., 1981, ApJ 250, 34
Linke A.R., Goldsmith P.F., 1980, ApJ 235, 437
Liszt H.S., Linke R.A., 1975, ApJ 196, 709
Little L.T., Gibb A.G., Heaton B.D., Elisson B.N., Claude S.M.X., 1990, MNRAS 271, 649
Lovas F.J., 1992, J. Phys. Chem. Ref. Data 21, 181
Margulis M., Snell R.L., 1988, ApJ 333, 316
Matthews N., Andersson M., MacDonald G.H., 1986, A&A 155, 99
Matthews N., Little L.T., MacDonald G.H., et al., 1987, A&A 184, 284
Menten K.M., 1987, Ph.D. Thesis, Bonn University
Menten K.M., 1991, ApJ 380, L175
Morgan J.A., Bally J., 1991, ApJ 372, 505
Mundy L.G., Evans N.J. II, Snell R.L., Goldsmith P.F., Bally J., 1986, ApJ 306, 670
Ohashi N., Kawabe R., Hayashi M., Ishiguro M., 1991, AJ 102, 2054
Pastor J., Estalella R., López R., et al., 1991, A&A 252, 320
Plambeck R.L., Menten K.M., 1990, ApJ 364, 555
Plume R., Jaffe D.T., Evans N.J., 1992, ApJS 78, 505
Plume R., Jaffe D.T., Evans N.J. II, Martín−Pintado J., Gómez−González J., 1997, ApJ 476, 730
Pratap P., Menten K., 1992, in: Astrophysical Masers, Clegg and Nedoluha (eds.). Springer Verlag, Berlin, Lecture Notes in Physics 412, 215
Rodríguez L.F., Moran J.M., Ho P.T.P, Gottlieb E.W., 1980, ApJ 235, 845
Rodríguez L.F., Carral P., Ho P.T.P., Moran J.M., 1982, ApJ 260, 635
Schwartz P.R., Gee G., Huang Y.L., 1988, ApJ 327, 350
Scoville N.Z., Sargent A.I., Sanders D.B., et al., 1986, ApJ 303, 416
Slysh V.I., Kalenskii S.V., Val'tts I.E., 1993, ApJ 413, L133
Slysh V.I., Bachiller R., Berulis I.I., et al., 1994, AZh 73, 37
Slysh V.I., Kalenskii S.V., Val'tts I.E., et al., 1998, A&A (in preparation)
Snell R.L., Langer W.D., Frerking M.A., 1982, ApJ 255, 149
Snell R.L., Goldsmith P.F., Erickson N.R., Mundy L.G., Evans N.J. II, 1984, ApJ 276, 625

Snell R.L., Huang Y.L., Dickman R.L., Claussen M.J., 1988, ApJ 325, 853
Snell R.L., Dickman R.L., Huang Y.L., 1990, ApJ 352, 139
Solomon, P.M., Rivolo, A.R., Barrett, J., Yahil, A., 1987, ApJ 319, 730
Stier M.T., Jaffe D.T., Rengarajan N.T., et al., 1984, ApJ 283, 573
Thronson H.A., Lada C.J., 1984, ApJ 284, 135
Turner B.E., Zuckerman B., Palmer P., Morris M., 1973, ApJ 186, 123
Wilking B.A., Blackwell J.H., Mundy L.G., 1990, AJ 100, 758
Waller W.H., Clemens D.P., Sanders D.B., Scoville N.Z., 1987, ApJ 314, 397
Wolf-Chase G.A., Walker C.K., Lada C.J., 1995, ApJ 442, 197
Wouterloot J.G.A., Henkel C., Walmsley C.M., 1989, A&A 215, 131
Wu Y., Huang M., He J., 1996, A&AS 115, 283
Xiang D., Turner B.E., 1995, ApJS 99, 121
Zheng X.W., Ho P.T.P., Reid M.J., Schneps M.H., 1985, ApJ 293, 522
Zhou Sh., Evans N.J., Güsten R., Mundy L.G., Kutner M.L., 1991, ApJ 372, 518
Zinchenko I., Forsström V., Lapinov A., Mattila K., 1994, A&A 288, 601